Ecole Evry Schatzman 2010: Star Formation in the Local Universe
Eds. C. Charbonnel & T. Montmerle
EAS Publications Series, 2011

STAR FORMATION ON GALACTIC SCALES: EMPIRICAL LAWS

Bruce G. Elmegreen[1]

Abstract. Empirical star formation laws from the last 20 years are reviewed with a comparison to simulations. The current form in main galaxy disks has a linear relationship between the star formation rate per unit area and the molecular cloud mass per unit area with a timescale for molecular gas conversion of about 2 Gyr. The local ratio of molecular mass to atomic mass scales nearly linearly with pressure, as determined from the weight of the gas layer in the galaxy. In the outer parts of galaxies and in dwarf irregular galaxies, the disk can be dominated by atomic hydrogen and the star formation rate per unit area becomes directly proportional to the total gas mass per unit area, with a consumption time of about 100 Gyr. The importance of a threshold for gravitational instabilities is not clear. Observations suggest such a threshold is not always important, while simulations generally show that it is. The threshold is difficult to evaluate because it is sensitive to magnetic and viscous forces, the presence of spiral waves and other local effects, and the equation of state.

1 Introduction: the Kennicutt-Schmidt law of Star Formation

Star formation and stellar evolution are such important drivers of galactic evolution that empirical laws to determine the star formation rate have been investigated for over 50 years. The results have never been very precise because star formation spans a wide range of scales, from cluster-forming cores to molecular clouds to the whole interstellar medium.

On the scale of a galaxy, the first idea was a proposed connection between the total star formation rate and the mass of interstellar gas. Schmidt (1959) derived the star formation rate (SFR) over the history of the Milky Way assuming a constant initial luminosity function for stars, $\Psi(M_{\rm V})$, a stellar lifetime function $T(M_{\rm V})$, a gas return per star equal to all of the stellar mass above 0.7 $M_\odot$, and a

[1] IBM T. J. Watson Research Center, 1101 Kitchawan Road, Yorktown Heights, New York 10598 USA, bge@us.ibm.com

DOI: (will be inserted later)

star formation rate $f(t)$ that scales with a power n of the gas mass, $M_{\rm G}(t)$. Then $f(t)\Sigma_{\rm MV}\Psi(M_{\rm V}) = C[M_{\rm G}(t)]^n$, for a summation $\Sigma_{\rm MV}$ over all stellar types.

Schmidt gave analytical solutions for $n = 0, 1, 2$. He noted that a scale height for HI of 144 pc, a scale height for Cepheids of 80 pc, and a scale height for clusters of 58 pc gave $n = 2$ to 3. The white dwarf count gave $n > 2$, the He abundance suggested $n = 2$, the uniformity of HI suggested $n \geq 2$, and the cluster mass function gave $n = 1$ to 2. Schmidt also suggested that with $n = 2$, dense galaxies like ellipticals should now have less gas than low-density galaxies like the LMC. His final comment was "It is hoped to study the evolution of galaxies in more detail in the future." Following Schmidt (1959), many authors derived scaling relations between the average surface density of star formation, $\Sigma_{\rm SFR}$, and the average surface density of gas. Buat, Deharveng & Donas (1989) included molecular and atomic gas and determined star formation rates from the UV flux corrected for Milky Way and internal extinction. They assumed a constant H_2/CO ratio and a Scalo (1986) IMF. The result was a good correlation between the average star formation rate in a sample of 28 galaxies and the 1.65 ± 0.16 power of the average total gas surface density. In the same year, Kennicutt (1989) used Hα for star formation, and HI and CO for the gas with a constant H_2/CO conversion factor, and determined star formation rates both as a function of galactocentric radius and averaged over whole galaxy disks. For whole galaxies, the average Hα flux scaled with the average gas surface density to a power between 1 and 2; there was a lot of scatter in this relation and the correlation was better for HI than H_2. More interesting was Kennicutt's (1989) result that the star formation rate had an abrupt cutoff in radius where the Toomre (1964) stability condition indicated the onset of gravitationally stable gas. Kennicutt derived a threshold gas column density for star formation, $\Sigma_{\rm crit} = \alpha\sigma\kappa/(3.36G)$ for $\alpha = 0.7$; σ is the velocity dispersion of the gas; κ is the epicyclic frequency, and G is the gravitational constant.

In a second study, Kennicutt (1998) examined the disk-average star formation rates using a larger sample of galaxies with Hα, HI, and CO. He found that for normal galaxies, the slope of the SFR-surface density relation ranged between 1.3 to 2.5, depending on how the slope was measured; there was a lot of scatter. When starburst galaxies with molecular surface densities in excess of 100 $M_\odot$ were included, the overall slope became better defined and was around 1.4. This paper also found a good correlation with a star formation rate that scaled directly with the average surface density of gas and inversely with the rotation period of the disk. This second law suggested that large-scale dynamical processes are involved.

Hunter et al. (1998) considered the same type of analysis for dwarf Irregulars and derived a critical surface density that was lower than the Kennicutt (1989) value by a factor of ~ 2. This meant that stars form in more stable gas in dwarf irregulars compared to spirals.

Boissiet et al. (2003) compared $\Sigma_{\rm SFR}$ and $\Sigma_{\rm gas}$ versus radius in 16 resolved galaxies with three theoretical expressions. The best fits were a SFR dependence on the gas surface density as $\Sigma_{\rm SFR} \propto \Sigma_{\rm gas}^{2.06}$, a more dynamical law from Boissier & Prantzos (1999) which gave the fit $\Sigma_{\rm SFR} \propto \Sigma_{\rm gas}^{1.48}(V/R)$ for rotation

speed V and radius R, and a third type of law from Dopita & Ryder (1994), which fit to $\Sigma_{\rm SFR} \propto \Sigma_{\rm gas}^{0.97}/\Sigma_{\rm tot}^{0.61}$. Boissiet et al. (2003) assumed that H_2/CO varied with radius as the metallicity (Boselli et al., 2002). Their conclusion was that the three laws are equally good, and that for the pure gas law, $n > 1.4$. Boissiet et al. (2003) also looked for a star formation threshold in the Milky Way. They determined $\Sigma/\Sigma_{\rm crit}$ using both pure-gas for $\Sigma_{\rm crit}$ and a gas+star $\Sigma_{\rm crit}$ from Wang & Silk (1994). They found that the gas+star $\Sigma_{\rm crit}$ gave the best threshold for determining where star formation occurs. The gas alone was sub-threshold throughout the disk.

Zasov & Smirnova (2005) showed that a threshold like $\Sigma_{\rm crit}$ may be used to determine the gas fraction in galaxies. If all galaxies have Σ(HI) approximately at the critical $\Sigma_{\rm crit} = \alpha\kappa\sigma/\pi G$, which is proportional to V/R from κ, then $M_{\rm gas} = \int_R 2\pi R\Sigma_{\rm crit} dR \propto VR$. This was shown to be the case from observations. They also considered that the total mass is $M_{\rm tot} \propto V^2 R$, in which case $M_{\rm tot}/M_{\rm gas} \propto V$, the rotation speed. This was also shown to be confirmed by observations. In their interpretation, small galaxies are more gas-rich than large galaxies because all galaxies have their gas column densities close to the surface density threshold.

For the Milky Way, Misiriotis et al. (2006) used COBE/DIRBE observations to get both the gas and dust distributions and the SFR distribution. They found a gas-law slope of 2.18 ± 0.20, which they claimed was similar to Kennicutt's (1998) bivariate fit slope $n = 2.5$ for normal galaxies. Luna et al. (2006) determined the Milky Way SFR from IRAS point sources and the CO surface density from a southern hemisphere survey (assuming constant H_2/CO). They found star formation concentrated in low-shear spiral arms and suggested an additional dependence on shear. Overall they derived $\Sigma_{\rm SFR} \sim \Sigma_{\rm gas}^{1.2\pm0.2}$. Vorobyov (2003) also suggested a shear dependence for the SFR based on observations of the Cartwheel galaxy, where there is an inner ring of star formation with high shear that is too faint for the normal Kennicutt law, given the gas column density.

1.1 The Q Threshold

A threshold for gravitational instabilities in rotating disks has been derived for various ideal cases. For an infinitely thin disk of isothermal gas, the dispersion relation for radial waves is $\omega^2 = k^2\sigma^2 - 2\pi G\Sigma k + \kappa^2$. Solving for the fastest growth rate ω gives the wavenumber at peak growth, $k = \pi G\Sigma/\sigma^2$, and the wavelength, $\lambda = 2\sigma^2/G\Sigma$, which is on the order of a kiloparsec in main galaxy disks. The dominant unstable mass is $M \sim (\lambda/2)^2\Sigma = \sigma^4/G^2\Sigma \sim 10^7\ M_\odot$ in local spirals. The peak rate is given by

$$\omega_{peak}^2 = -(\pi G\Sigma/\sigma^2)^2 + \kappa^2 = -(\pi G\Sigma/\sigma^2)^2(1 - Q^2) \qquad (1.1)$$

which requires $Q \equiv \kappa\sigma/\pi G\Sigma < 1$ for instability (i.e., when $\omega_{peak}^2 < 0$).

Disk thickness weakens the gravitational force in the in-plane direction by an amount that depends on wavenumber, approximately as $1/(1+kH)$ for exponential scale height H (e.g., Elmegreen, 1987; Kim & Ostriker, 2007). Typically, $k \sim 1/H$, so this weakening can slow the instability by a factor of ~ 2, and it can make

the disk slightly more stable by a factor of 2 in Q. On the other hand, cooling during condensation decreases the effective value of the velocity dispersion, which should really be written $\gamma^{1/2}\sigma$ for adiabatic index γ that appears in the relation $\delta P \propto \delta\rho^{\gamma}$ with pressure P and density ρ. If P is nearly constant for changes in ρ, as often observed, then $\gamma \sim 0$. Myers (1978) found $\gamma \sim 0.25$ for various thermal temperatures at interstellar densities between 0.1 cm^{-3} and 100 cm^{-3}. Thus the effects of disk thickness and a soft equation of state partially compensate for each other.

There is also a Q threshold for the collapse of an expanding shell of gas (Elmegreen, Palous & Ehlerova, 2002). Pressures from OB associations form giant shells of gas and cause them to expand. Eventually they go unstable when the accumulated gas is cold and massive enough, provided the induced rotation and shear from Coriolis forces are small. Considering thousands of initial conditions, these authors found that a sensitive indicator of whether collapse occurs before the shell disperses is the value of Q in the local galaxy disk, i.e., independent of the shell itself. The fraction f of shells that collapsed scaled inversely with Q as $f \sim 0.5 - 0.4 \log_{10} Q$.

The Toomre Q parameter is also likely to play a role in the occurrence of instabilities in turbulence-compressed gas on a galactic scale (Elmegreen, 2002). Isothermal compression has to include a mass comparable to the ambient Jeans mass, $M_{\rm Jeans}$, in order to trigger instabilities. The turbulent outer scale in the galaxy is comparable to the Jeans length, $L_{\rm Jeans}$, which is about the galactic gas scale height, H. If the compression distance exceeds the epicyclic length, then Coriolis forces spin up the compressed gas, leading to resistance from centrifugal forces. So instability needs $L_{\rm Jeans} \le L_{\rm epicycle}$, which means $Q \le 1$, since $L_{\rm Jeans} \sim H \sim \sigma^2/\pi G\Sigma$. The epicyclic length is $L_{\rm epicycle} \sim \sigma/k$, so $L_{\rm Jeans}/L_{\rm epicycle} = Q$.

The dimensionless parameter Q measures the ratio of the centrifugal force from the Coriolis spin-up of a condensing gas perturbation to the self-gravitational force, on the scale where gravity and pressure forces are equal, which is the Jeans length. The derivation of Q assumes that angular momentum is conserved, so the Coriolis force spins up the gas to the maximum possible extent. When $Q > 1$, a condensing perturbation on the scale of the Jeans length spins up so fast that its centrifugal force pulls it apart against self-gravity. Larger-scale perturbations have the same self-gravitational acceleration (which scales with Σ) and stronger Coriolis acceleration (which scales with κ^2/k); smaller-scale perturbations have stronger accelerations from pressure. If angular momentum is not conserved, then the disk can be unstable for a wider range of Q because there is less spin up during condensation. For example, the Coriolis force can be resisted by magnetic tension or viscosity and then the angular momentum in a condensing cloud will get stripped away. This removes the Q threshold completely (Chandrasekhar, 1954; Stephenson, 1961; Lynden-Bell, 1966; Hunter & Horak, 1983). In the magnetic case, the result is the Magneto-Jeans instability, which can dominate the gas condensation in low-shear environments like spiral arms and some inner disks (Elmegreen, 1987, 1991, 1994; Kim & Ostriker, 2001, 2002; Kim et al., 2002). For the viscous case, Gammie (1996) showed that for Q close to but larger than 1, i.e.,

in the otherwise stable regime, viscosity can make the gas unstable with a growth rate equal to nearly one-third of the full rate for a normally unstable ($Q < 1$) disk. A dimensionless parameter for viscosity ν is $\nu\kappa^3/G^2\Sigma^2$, which is ~ 11 according to Gammie (1996). This is a large value indicating that galaxy gas disks should be destabilized by viscosity. An important dimensionless parameter for magnetic tension is $B^2/(\pi G\Sigma^2) \sim 8$, which is also large enough to be important. Thus gas disks should be generally unstable to form small spiral arms and clouds, even with moderately stable Q, although the growth rate can be low if Q is large.

1.2 Modern Versions of the KS Law with ~ 1.5 *slope*

Kennicutt et al. (2007) studied the local star formation law in M51 with 0.5-2 kpc resolution using Pa-α and 24μ+Hα lines for the SFR, and a constant conversion factor for CO to H_2. There was a correlation, mostly from the radial variation of both SFR and gas surface density, with a slope of 1.56 ± 0.04. There was no correlation with Σ(HI) alone, as this atomic component had about constant column density ($\sim 10\ M_\odot$). The correlation with molecules alone was about the same as the total gas correlation.

Leroy et al. (2005) studied dwarf galaxies and found that they have a molecular KS index of 1.3 ± 0.1, indistinguishable from that of spirals, except with a continuation to lower central H_2 column densities (i.e., down to $\sim 10\ M_\odot\ \mathrm{pc}^{-2}$).

Heyer et al. (2004) found a slope $n = 1.36$ for $\Sigma_{\rm SFR}$ versus $\Sigma(H_2)$ in M33, where the molecular fraction, $f_{\rm mol}$ is small. The correlation with the total gas was much steeper. More recently, Verley et al. (2010) studied M33 again and got $\Sigma_{\rm SFR} \propto \Sigma_{\rm H2}^n$ for $n = 1$ to 2, and $\Sigma_{\rm SFR} \propto \Sigma_{\rm total\ gas}^n$ for $n = 2$ to 4. The steepening for total gas is again because $\Sigma_{\rm HI}$ is about constant, so the slope from HI alone is nearly infinite. This correlation is dominated by the radial variations in both quantities, as it is a point-by-point evaluation throughout the disk. Radial changes in metallicity, spiral arm activation, tidal density, and so on, are part of the total correlation. Verley et al. (2010) also try other laws, such as $\Sigma_{\rm SFR} \propto \left(\Sigma_{\rm H2}\rho_{\rm ISM}^{0.5}\right)^n$, for which $n = 1.16 \pm 0.04$, and $\Sigma_{\rm SFR} \propto \rho_{\rm ISM}^n$, for which $n = 1.07 \pm 0.02$. These differ by considering the conversion from column density to midplane density, using a derivation of the gaseous scale height. The first of these would have a slope of unity if the star formation rate per unit molecular gas mass were proportional to the dynamical rate at the average local (total) gas density. The second has the form of the original Schmidt law, which depends only on density. To remove possible effects of CO to H_2 conversion, Verley et al. also looked for a spatial correlation with the 160 μ opacity, τ_{160}, which is a measure of the total gas column density independent of molecule formation. They found $\Sigma_{\rm SFR} \propto \tau_{160}^n$ for $n = 1.13 \pm 0.02$, although the correlation was not a single power law but a 2-component power law with a shallow part (slope ~ 0.5) at low opacity ($\tau_{160} < 10^{-4}$) and a steep part (slope ~ 2) at high opacity.

1.3 Explanations for the 1.5 slope

Prior to around 2008, the popular form of the KS law had a slope of around 1.5 when $\Sigma_{\rm SFR}$ was plotted versus total gas column density on a log-log scale. This follows from a dynamical model of star formation in which the SFR per unit area equals the available gas mass per unit area multiplied by the rate at which this gas mass gets converted into stars, taken to be the dynamical rate,

$$\Sigma_{\rm SFR} \sim \epsilon \Sigma_{\rm gas} \left(G \rho_{\rm gas}\right)^{1/2} . \tag{1.2}$$

If the gas scale height is constant, then $\Sigma_{\rm gas} \propto \rho_{\rm gas}$ and $\Sigma_{\rm SFR} \propto \Sigma_{\rm gas}^{1.5}$. In the model of star formation where star-forming clouds are made by large-scale gravitational instabilities, this 1.5 power law would work only where the Toomre instability condition, $Q \leq 1.4$, is satisfied. Such a model accounts for the Kennicutt (1989, 1998) law with the $Q < 1.4$ threshold.

Several computer simulations have shown this dynamical effect. Li et al. (2006) did SPH simulations of galaxy disks with self-gravity forming sink particles at densities larger than 10^3 cm^{-3}. They found a Q threshold for sink particle formation, and had a nice fit to the KS law with a slope of ~ 1.5. Tasker & Bryan (2006) ran ENZO, a 3D adaptive mesh code, with star formation at various efficiencies, various temperature floors in the cooling function, and various threshold densities. Some models had a low efficiency with a low threshold density and other models had a high efficiency with a high threshold density. Some of their models had feedback from young stars. They also got a KS slope of ~ 1.5 for both global and local star formation, regardless of the details in the models. Kravtsov (2003) did cosmological simulations using N-body techniques in an Eulerian adaptive mesh. He assumed a constant efficiency of star formation at high gas density, and star formation only in the densest regions ($n > 50$ cm^{-3}, the resolution limit), which are in the tail of the density probability distribution function (pdf; cf. Elmegreen, 2002; Krumholz & McKee, 2005). Kravtsov (2003) got the KS law with a slope of 1.4 for total gas surface density. Wada & Norman (2007) did a similar thing, using the fraction of the mass at a density greater than a critical value from the pdf ($\rho_{\rm crit} = 10^3$ cm^{-3}) to determine the star formation rate. Their analytical result had a slope of 1.5. Harfst, Theis & Hensler (2006) had a code with a hierarchical tree for tracking interacting star particles, SPH for the diffuse gas, and sticky particles for the clouds. They included mass exchange by condensation and evaporation, mass exchange from stars to clouds (via PNe) and from stars to diffuse gas (SNe), and from clouds into stars during star formation. New clouds were formed in expanding shells. Their KS slope was 1.7 ± 0.1. They also got a drop in $\Sigma_{\rm SFR}$ at low $\Sigma_{\rm gas}$, not from a Q threshold but from an inability of the gas to cool and form a thin disk (cf. Burkert et al., 1992; Elmegreen & Parravano, 1994).

2 The Molecular Star Formation Law

The star formation law may also be written as a linear relation for molecules, with $\Sigma_{\rm SFR} \propto \Sigma_{\rm H2}^1$ (e.g., Rownd & Young, 1999). Wong & Blitz (2002) found a SFR in

direct proportion to molecular cloud density ($n = 1$), and suggested that the $n = 1.4$ KS law came from changes in the molecular fraction, $f_{\rm mol} = \Sigma_{\rm H2}/\left(\Sigma_{\rm HI} + \Sigma_{\rm H2}\right)$. They assumed that H_2/CO was constant and determined the combined index $n' = n_{\rm mol}\left(1 + d\ln f_{\rm mol}/d\ln\Sigma_{\rm gas}\right)$ where $n_{\rm mol} = 1$ and $f_{\rm mol}$ increases with pressure, P. They measured $d\ln f_{\rm mol}/d\ln P \sim 0.2$, and if $P \propto \Sigma_{\rm gas}^2$, then $d\ln f_{\rm mol}/d\ln\Sigma_{\rm gas} \sim 0.4$. This gives the KS $n = 1.4$ law for total gas. Wong & Blitz also suggested that the stability parameter Q was not a good threshold for star formation, but a better measure of the gas fraction in the sense that a high Q corresponds to a low $\Sigma_{\rm gas}/\Sigma_{\rm tot}$. Blitz & Rosolowski (2006) showed for a wider sample of 13 galaxies that the molecular ratio, $R_{\rm mol} = \Sigma_{\rm H2}/\Sigma_{\rm HI}$, scales about linearly with the total ISM pressure. Interacting galaxies had slightly higher $R_{\rm mol}$ for a given P, but among interacting galaxies, the correlation was still present.

A large study of HI, CO, and star formation rates from GALEX ultraviolet and Spitzer 24μ observations was made by Bigiel et al. (2008) and Leroy et al. (2008). They considered the local star formation law with a resolution of 750 pc. Bigiel et al. found that $\Sigma_{\rm SFR} \propto \Sigma_{\rm CO}$, and that the timescale for conversion from H_2 to stars was about 2 Gyr. Figure 1 (from Bigiel et al., 2008) shows an example of how much better the SFR scales with CO than either HI or the total gas. The CO and SFR maps of NGC 6946 resemble each other closely, and neither resembles the HI map. Bigiel et al. also found that $\Sigma_{\rm HI}$ saturates to $\sim 9\ M_\odot\ {\rm pc}^{-2}$. When plotting $\Sigma_{\rm SFR}$ over a wide range of $\Sigma_{\rm HI+H2}$, they found a slope of unity in the molecular range, $\Sigma_{\rm HI+H2} > 9\ M_\odot\ {\rm pc}^{-2}$, and higher slope in the atomic range ($\Sigma_{\rm HI+H2} < 9\ M_\odot\ {\rm pc}^{-2}$). Figure 2 shows the summed distribution of SFR per unit area versus total gas column density in 7 spiral galaxies. There is a linear part at high column density and a steeper part at low column density.

Dwarf galaxies look like the outer parts of spirals in the Bigiel et al. survey, occupying the steeper part of the $\Sigma_{\rm SFR} - \Sigma_{\rm gas}$ diagram at low $\Sigma_{\rm gas}$. At higher $\Sigma_{\rm HI+H2}$, the survey did not have new data, but Bigiel et al. suggested, based

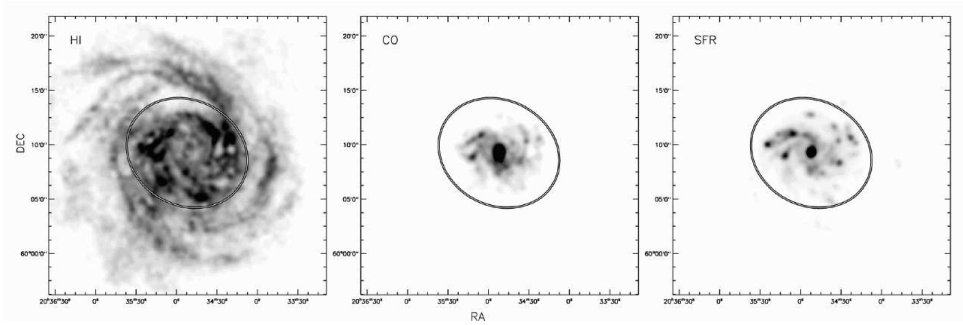

Fig. 1. Maps of HI, CO and SFR in NGC 6946 with HI on the left, CO in the middle and SFR on the right, all convolved to 750 pc resolution (from Bigiel et al. (2008). The circle is the optical radius at 25 mag arcsec^{-2}.

on Kennicutt's (1998) starburst result, that perhaps the KS law turned up to a steeper slope ($n \sim 1.4$) in a third regime of star formation where $\Sigma_{\rm H2}$ exceeds the standard column density of a single molecular cloud (around 100 $M_\odot$ pc^{-2}).

Leroy et al. (2008) compared these new survey results to various theoretical models. They found that the star formation time in CO-rich gas is universally 1.9 Gyr, independent of the average local free fall or orbital time, the midplane gas pressure, the state of gravitational stability of the disk with or without the inclusion of stars in the stability condition, and regardless of the rate of shear or the ability of a cold gas phase to form. Star formation depends only on the presence of molecules and it proceeds at a fixed rate per molecule. Leroy et al. also found that dwarf galaxies are forming stars at their average historical rate, whereas spirals are forming stars at about half of their average rate. In the outer disk, the SFR in HI drops with radius faster than the free fall time, suggesting self-gravity is not the lone driver. Also important are the phase balance between HI and H_2, giant molecular cloud (GMC) destruction, stellar feedback, and other processes. These processes govern the presence of GMCs with an apparently constant star formation efficiency in each GMC.

Unlike the star formation rate per molecule, the molecule-to-atom ratio does

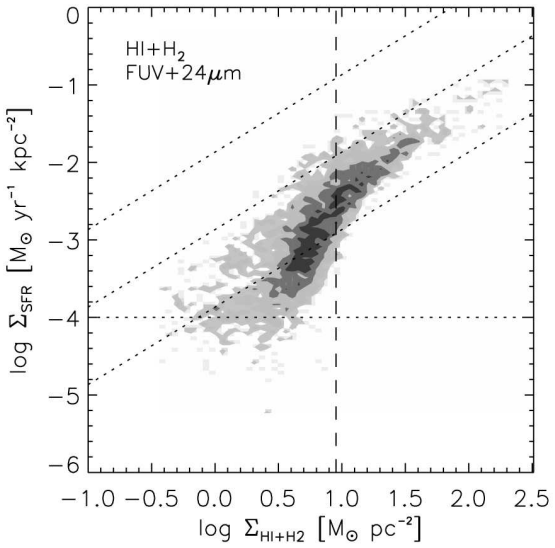

Fig. 2. The distribution of SFR per unit area versus total gas column density, convolved to 750 pc, for 7 spiral galaxies (from Bigiel et al. (2008). There is a change in the slope from ~ 4 at $\Sigma_{\rm HI+H2} < 9$ $M_\odot$ pc^{-2} (the vertical dashed line) in the outer disk to ~ 1 at higher $\Sigma_{\rm HI+H2}$ in the inner disk. The short-dashed lines correspond to gas depletion times of 0.1 Gyr, 1 Gyr, and 10 Gyr, from top to bottom.

correlate well with environmental parameters. Leroy et al. (2008) showed approximately linear correlations with stellar surface density and interstellar pressure, an inverse squared dependence on the orbit time, and an exponential dependence on the galactic radius, like the rest of the disk, and with a comparable radial scale length. The molecular fraction is a smooth function of environmental parameters (e.g., pressure); no thresholds were seen. Disks seem to be marginally stable throughout.

Leroy et al. concluded by noting that the HI-H_2 transition in spirals typically occurs at $0.43 \pm 0.18\ R_{25}$, which is about the same as where $\Sigma_{\rm stars} = 81 \pm 25\ M_\odot\ {\rm pc}^{-2}$, $\Sigma_{\rm gas} = 14 \pm 6\ M_\odot\ {\rm pc}^{-2}$, $P = 2.3 \pm 1.5 \times 10^4 k_{\rm B}$ K cm^{-3}, and $T_{\rm orbit} = 1.8 \pm 0.4$ Gyr. There should be unobserved H_2 in dwarfs, according to the high star formation rates and low CO emissions there; in fact Leroy et al. estimate for dwarfs $\Sigma_{\rm H2} \sim 2\Sigma_{\rm HI}$ in the inner regions.

Where $\Sigma_{\rm HI} > \Sigma_{\rm H2}$, the star formation efficiency is proportional to $\Sigma_{\rm stars}$, making

$$\Sigma_{\rm SFR} \sim \Sigma_{\rm gas} \times \left[\Sigma_{\rm stars}/81\ M_\odot\ {\rm pc}^{-2}\right]/1.9\ {\rm Gyr}. \tag{2.1}$$

2.1 Theoretical Models for the Bigiel-Leroy Observations

Krumholz et al. (2008) considered the molecule formation problem by starting with the radiative transfer of H_2-dissociating radiation: $dF/dz = -n\sigma_{\rm d}F - f_{\rm HI}n^2R/f_{\rm diss}$. Here, F is the flux in Lyman-Werner bands that dissociate H_2, n is the density (~ 30 cm^{-3} near the H_2 transition), $\sigma_{\rm d}$ is the dust cross section per H (10^{-21} cm^2), $f_{\rm HI}$ is the fraction of n that is HI, R is the rate coefficient for formation of H_2 on grains ($\sim 3 \times 10^{-17}$ cm^3 s^{-1}; i.e., the formation rate is $f_{\rm HI}n^2R$), and $f_{\rm diss}$ is the fraction of uv photon absorptions that dissociate H_2 (~ 0.1).

The solution to this radiative transfer equation is $F(\tau) = \left(e^{-[\tau-\tau_{\rm HI}]} - 1\right)/\chi$ where $\tau_{\rm HI} = \ln(1+\chi)$; $\chi = f_{\rm diss}\sigma_{\rm d}cE_0/nR$ is the ratio of absorption in dust to H_2, and E_0 is the free space photon number density ($\sim 7.5 \times 10^{-4}$ cm^{-3}). Krumholz et al. (2008) assume that the cold neutral density comes from two phase equilibrium. Then n scales with E_0 and χ becomes nearly constant. From this they get the extinction, $A_{\rm V}$, to the HI/H_2 transition, the HI column density, $\Sigma_{\rm HI}$, and the molecular fraction in spherical cloud complexes as a function of the complex total column density. They do this also as a function of metallicity.

After considering a galactic cloud population, Krumholz et al. (2009a) derive $\Sigma_{\rm HI}$ versus $\Sigma_{\rm total\ gas}$ for different metallicities, and compare this with observations of galaxies having those metallicities. They do the same for H_2. They also compare the observed versus the predicted correlation between H_2/HI and pressure P. To do this, they use the observed $\Sigma_{\rm total\ gas}$ and metallicity, and then compute $R_{\rm H2} = \Sigma_{\rm H_2}/\Sigma_{\rm HI}$ from theory. This is plotted versus the observed pressure from Blitz & Rosolowski (2006) and Leroy et al. (2008). The agreement is good.

Krumholz et al. (2009b) considered the star formation law,

$$\Sigma_{\rm SFR} = \Sigma_{\rm gas} f_{\rm H2} SFR_{\rm ff}/t_{\rm ff} \tag{2.2}$$

where the star formation rate in a free fall time is the fraction of the gas that turns into stars in a free fall time, $SFR_{\rm ff}$, divided by the free fall time, $t_{\rm ff}$. This is $SFR_{\rm ff}/\tau_{\rm ff} = (M_6^{-0.33}/0.8\ {\rm Gyr}) \times {\rm Max}[1, \Sigma_{\rm gas}/85\ M_\odot\ {\rm pc}^{-2}]$; M_6 is the cloud mass in units of $10^6\ M_\odot$. This equation assumes that stars form in the high density tail of a log-normal density pdf, with the tail width given by the Mach number; a fraction of 0.3 of the dense gas mass goes into stars. The clouds are virialized and at uniform pressure until the galactic $\Sigma_{\rm gas}$ exceeds the column density of a single GMC; then the pressure equals the galactic pressure. Also, the cloud complex mass is taken to be $M_6 = 37\Sigma_{\rm gas}/(85\ M_\odot\ {\rm pc}^{-2})$ from the galaxy Jeans mass.

This theory for molecule formation and star formation in a galactic environment fits well to the observations by Bigiel et al. (2008) and Leroy et al. (2008). It reproduces the low column density regime by having a low ratio of molecules to atoms at low pressure, it reproduces the intermediate column density regime by having a fixed star formation rate per molecule and an areal average star formation rate from the areal density of molecular clouds at constant pressure, and it reproduces the high column density regime by increasing the interstellar pressure, which makes the cloud density go up and the free fall time go down. A key point in their model is that molecular cloud pressures are constant in normal galaxy disks because they are set by HII region pressures (feedback) and not the galactic environment. In this sense, all GMCs have to be parts of shells or other active disturbances formed by high pressures.

We know that molecular cloud pressures in the Milky Way are about constant from the Larson (1981) laws, which require this for virialized clouds, but we don't really know the reason for it. It could be feedback, as Krumholz et al. (2009b) suggest, or it could be the weight of the HI shielding layer, which has a regulatory effect on pressure (Elmegreen, 1989). This regulatory effect works because at high ambient pressure, the atomic density on the periphery of molecular clouds is high and so the required surface column density for H_2 line self-shielding is low, and vice versa. The pressure at the bottom of the shielding layer, which is the molecular cloud surface pressure, scales directly with the column density of the shielding layer. Thus a lower intercloud pressure is compensated by a higher HI column density at the molecular cloud surface, making the molecular cloud surface pressure somewhat uniform.

Robertson & Kravtsov (2008) simulated star formation in galaxies. They took a star formation rate per unit volume

$$d\rho_{\rm stars}/dt = f_{\rm H2} \times (\rho_{\rm gas}/t_{\rm SF}) \times (n_{\rm H}/[10\ {\rm cm}^{-3}])^{0.5} \qquad (2.3)$$

where $t_{\rm SF} = t_{\rm ff}/\epsilon_{\rm ff}$ is the free fall time, $t_{\rm ff}$, divided by the fraction of the gas that turns into stars in a free fall time, $\epsilon_{\rm ff} = 0.02$. To determine the molecular fraction, $f_{\rm H2}$, they considered heating and cooling, a radiation field proportional to the SFR, the Sternberg, et al. (2002) H_2 formation theory, and radiative transfer using the *Cloudy* code. The result was a SFR that scaled steeply with the total gas column density, as observed, a higher KS slope for lower mass galaxies, which is also observed, and a shallower KS slope for the H_2 column density alone, as in the molecular KS law. These results were somewhat independent of galaxy

mass. The molecular/atomic ratio also scaled with pressure in an approximately linear fashion, regardless of galaxy mass, as observed. They also found a stability parameter Q that ranged from unstable in the inner, star-forming parts of the disk, to stable in the outer regions.

2.2 Observations and Models of Outer Disks

Murante et al. (2010) have a multi-phase SPH code that assumes pressure determines the molecular abundance, and the molecules give the SFR. Below $\Sigma_{\rm total\ gas} \sim 10\ M_\odot\ {\rm pc}^{-2}$, the slope of the molecular star formation law turns out to be very steep, $\Sigma_{\rm SFR} \propto \Sigma^n_{\rm total\ gas}$ for $n \sim 4$. Above $10\ M_\odot\ {\rm pc}^{-2}$, the slope is the same as in the Kennicutt law, $n = 1.4$, which is steeper than in Bigiel et al. (2008), where $n \sim 1$ for the molecular Schmidt law.

Bush et al. (2010) simulated galactic star formation with special attention to the outer disks. The star formation model followed Springel & Hernquist (2002) with radiative cooling, star formation in the cold phase, no specific molecular phase, and a volume-Schmidt law, $\rho_{\rm SFR} \propto \rho^{1.5}_{\rm total\ gas}$. They found patchy star formation in the outer parts, usually along spiral arcs where the gas density was high. This morphology is in agreement with GALEX observations (Thilker et al., 2005; Gil de Paz et al., 2005). The Bigiel et al. and Leroy et al. observations were matched qualitatively in these outer parts too: below $\Sigma_{\rm gas} \sim 10\ M_\odot\ {\rm pc}^{-2}$, the slope $n \sim 6$ to 8 was steeper than in the observations (which also plot SFR versus total gas in the outer regions). Then it was less steep at higher column density, with a slope of $n \sim 1.4$, which agrees with the Kennicutt (1998) slope for total gas.

Outer disks can be Toomre-stable on average because the gas and star column densities are very low. This is especially true for dwarf galaxies (Hunter et al., 1998). It might be that magnetic fields and viscosity destabilize outer disks, as discussed in Section 1.1, but in any case, outer disks appear to be much more stable than inner disks. More importantly, the gas is outer disks is often far from uniform and the use of an average column density for Q is questionable. Locally there can be islands of high column density where Q is small enough to be in the unstable region (van Zee et al., 1996). These islands have to be larger than the Jeans mass, which might be $10^7\ M_\odot$. Spiral arms and large disturbances in pressure could make unstable regions like this. Dong et al. (2008) found unstable islands of star formation in the outer part of M83. In these regions, the star formation followed a steep KS law from point to point with a slope of about 1.4 (Dong et al., 2008).

Bigiel et al. (2010a) found that outer disk star formation seen by GALEX follows the HI very well in M83, with a uniform consumption time of 100 Gyr per atom beyond $1.5R_{25}$. The form of the star formation is mostly in spiral arms. Outer disk arms could be spiral waves radiating from the inner disk (Bertin & Amorisco, 2010).

Boissier et al. (2008) observed the galaxy-integrated KS law in low surface brightness galaxies, using a SFR from GALEX NUV observations. For a given total HI mass, the star formation rate was low by a factor of ~ 5 compared to normal

spirals, but over the whole range, the total star formation rate scaled directly with the HI mass. This is not the same as saying that the star formation rate per unit area scales directly with the HI column density because the observations are spread out in a plot like this with big galaxies on one side and small galaxies on the other.

Bigiel et al. (2010b) studied SF rates in the far-outer disks of 17 spiral and 5 dwarf galaxies, where the gas is highly HI dominated. The SF laws compare well with those in dwarf galaxies. There is no obvious Q threshold. They suggest that the total SF Law has three components, the extreme outer disk component that is HI dominated, a transition region where the molecular fraction increases to near unity, the molecular region inside of that, and the starburst component, where the surface density is higher than that of a single GMC.

2.3 Scaling relations inside individual clouds

Krumholz & Tan (2007) showed that the conversion rate from gas to stars per unit free fall time is about constant inside clouds over a wide range of densities. This implies that the SFR per unit volume scales with the 1.5 power of density, with the first 1 in the power coming from the mass per unit volume, and the 0.5 in the power coming from the free fall rate. This is like a KS law, but for individual GMCs. There is also a threshold column density for star formation inside GMCs of around $\sim 5-7$ mag in V (Johnstone et al., 2004; Kirk et al., 2006; Enoch et al., 2006; Jørgensen et al., 2007).

Chen et al. (2010) studied the KS relation for individual GMCs in the LMC. They measured the star formation rate from both HII regions and by direct counting of young stellar objects. For YSO counting, the rate per unit area inside a cloud approximately satisfies the total-gas Kennicutt relation with the same time scale per atom, ~ 1 Gyr. For these regions, $\Sigma_{\rm HI+H_2} \sim 100\ M_\odot\ {\rm pc}^{-2}$, larger than in the main parts of galaxy disks. Chen et al. also found that the areal rate of star formation was much lower in the long molecular ridge south of 30 Doradus than in the GMCs. Presumably this ridge is not strongly self gravitating, even though it is CO-rich.

3 Summary

The empirical star formation law on kpc scales is essentially one where star formation follows CO-emitting molecular gas with a constant rate per molecule, and the ratio of molecular to atomic gas scales nearly directly with the ISM pressure (Bigiel et al., 2008; Leroy et al., 2008). The rate per molecule corresponds to a consumption time of molecular gas equal to about 2 Gyr. The place in a galaxy where the transition occurs between HI dominance in the outer part to H_2 dominance in the inner part is at a pressure of $P = 2.3 \pm 1.5 \times 10^4 k_{\rm B}$ K cm^{-3}. There also tend to be characteristic gas and stellar column densities at this place, and a characteristic galactic orbit time for all of the galaxies observed. Beyond this

radius is the atomic-dominated outer disk. There, the SFR scales directly with $\Sigma_{\rm HI}$, and the consumption time is about 100 Gyr.

Theoretical models of these empirical laws include the atomic-to-molecular transition in individual clouds and a sum over clouds to give the galactic scaling laws. Star formation occurs only in the densest parts of the clouds, as determined by a combination of turbulence-compression and self-gravity. Numerous simulations of star formation in galaxies can reproduce these empirical laws fairly well. The simulations usually show a sensitivity to the Toomre Q parameter, unlike the observations.

References

Bertin, G., & Amorisco, N. C. 2010, A&A, 512, 17

Bigiel, F., Leroy, A., Walter, F., Brinks, E., de Blok, W. J. G., Madore, B., & Thornley, M. D. 2008, AJ, 136, 2846

Bigiel, F., Leroy, A., Seibert, M., Walter, F., Blitz, L., Thilker, D., & Madore, B. 2010a, ApJ, 720, 31

Bigiel, F., Leroy, A., Walter, F., Blitz, L., Brinks, E., de Blok, W. J. G., & Madore, B. 2010b, arXiv1007.3498

Blitz, L., & Rosolowsky, E. 2006, ApJ, 650, 933

Boissier, S., & Prantzos, N. 1999, MNRAS, 307, 857

Boissier, S., Prantzos, N., Boselli, A., & Gavazzi, G. 2003, MNRAS, 346, 1215

Boissier, S., Gil de Paz, A., Boselli, A., Buat, V., Madore, B., Chemin, L., Balkowski, C., Amram, P., Carignan, C., & van Driel, W. 2008, ApJ, 681, 244

Boselli, A., Lequeux, J., & Gavazzi, G. 2002, A&A, 384, 33

Buat, V., Deharveng, J. M., & Donas, J. 1989, A&A, 223, 42

Burkert, A., Truran, J.W., & Hensler, G. 1992, ApJ, 391, 651

Bush, S.J., Cox, T. J., Hayward, C.C., Thilker, D., Hernquist, L., & Besla, G. 2010, ApJ, 713, 780

Chandrasekhar, S. 1954, ApJ, 119, 7

Chen, C.H.R. et al. 2010, arXiv1007.5326

Dong, H., Calzetti, D., Regan, M., Thilker, D., Bianchi, L., Meurer, G.R., & Walter, F. 2008, AJ, 136, 479

Dopita, M.A., & Ryder, S.D. 1994, ApJ, 430, 163

Elmegreen, B.G. 1987, ApJ, 312, 626

Elmegreen, B.G. 1989, ApJ, 338, 178

Elmegreen, B.G. 1991, ApJ, 378, 139

Elmegreen, B.G. 1994, ApJ, 433, 39

Elmegreen, B.G. 2002, ApJ, 577, 206

Elmegreen, B.G., & Parravano, A. 1994, ApJ, 435, L121

Elmegreen, B. G., Palous, J., & Ehlerova, S. 2002, MNRAS, 334, 693

Enoch, M.L. et al. 2006, ApJ, 638, 293

Gammie, C.F. 1996, ApJ, 462, 725

Gil de Paz, A., et al. 2005, ApJL, 627, 29

Guiderdoni, B. 1987, A&A, 172, 27

Harfst, S., Theis, Ch., & Hensler, G. 2006, A&A, 449, 506

Heyer, M.H., Corbelli, E., Schneider, S.E., & Young, J.S. 2004, ApJ, 602, 723

Hunter, D.A., Elmegreen, B.G., Baker, A.L. 1998, ApJ, 493, 595

Hunter, J.H., Jr. & Horak, T. 1983, ApJ, 265, 402

Johnstone, D., Di Francesco, J., & Kirk, H. 2004, ApJ, 611, L45

Jørgensen, J.K., Johnstone, D., Kirk, H., & Myers, P.C. 2007, ApJ, 656, 293

Kennicutt, R.C., Jr. 1989, ApJ, 344, 685

Kennicutt, R.C., Jr. 1998, ApJ, 498, 541

Kennicutt, R.C., Jr., et al. 2007, ApJ, 671, 333

Kim, W.-T., & Ostriker, E.C. 2001, ApJ, 559, 70

Kim, W.-T., & Ostriker, E.C. 2002, ApJ, 570, 132

Kim, W.-T., & Ostriker, E.C. 2007, ApJ, 660, 1232

Kim, W.-T., Ostriker, E.C., & Stone, J.M. 2002, ApJ, 581, 1080

Kirk, H., Johnstone, D., & Di Francesco, J. 2006, ApJ, 646, 1009

Kravtsov, A.V. 2003, ApJ, 590, L1

Krumholz, M.R., & McKee, C.F. 2005, ApJ, 630, 250

Krumholz, M.R., & Tan, J.C. 2007, ApJ, 654, 304

Krumholz, M.R., McKee, C.F., & Tumlinson, J. 2008, ApJ, 689, 865

Krumholz, M.R., McKee, C.F., & Tumlinson, J. 2009a, ApJ, 693, 216

Krumholz, M.R., McKee, C.F., & Tumlinson, J. 2009b, ApJ, 699, 850

Larson, R. B. 1981, MNRAS, 194, 809

Leroy, A., Bolatto, A. D., Simon, J. D., & Blitz, L. 2005, ApJ, 625, 763

Leroy, A.K., Walter, F., Brinks, E., Bigiel, F., de Blok, W. J. G., Madore, B., & Thornley, M. D. 2008, AJ, 136, 2782

Li, Y., Mac Low, M.-M., & Klessen, R.S. 2006, ApJ, 639, 879

Luna, A., Bronfman, L., Carrasco, L., & May, J. 2006, ApJ, 641, 938

Lynden-Bell, D. 1966, Observatory, 86, 57

Misiriotis, A., Xilouris, E. M., Papamastorakis, J., Boumis, P., & Goudis, C. D. 2006, A&A, 459, 113

Murante, G., Monaco, P., Giovalli, M., Borgani, S., & Diaferio, A. 2010, MNRAS, 405, 1491

Myers, P. C. 1978, ApJ, 225, 380

Robertson, B.E., & Kravtsov, A.V. 2008, ApJ, 680, 1083

Rownd, B.K., & Young, J.S. 1999, AJ, 118, 670

Scalo, J.M. 1986, Fund.Cos.Physics, 11, 1

Schmidt, M. 1959, ApJ, 129, 243

Springel, V., & Hernquist, L. 2002, MNRAS, 333, 649

Sternberg, A., McKee, C. F., & Wolfire, M. G. 2002, ApJS, 143, 419

Gil de Paz, A., et al. 2005, ApJ, 627, L29

Stephenson, G. 1961, MNRAS, 122, 455

Tasker, E.J., & Bryan, G.L. 2006, ApJ, 641, 878

Thilker, D. A., et al. 2005, ApJ, 619, L79

Toomre, A. 1964, ApJ, 139, 1217

van Zee, L., Haynes, M. P., Salzer, J. J., & Broeils, A. H. 1996, AJ, 113, 1618

Verley, S., Corbelli, E., Giovanardi, C., & Hunt, L. K. 2010, A&A, 510, 64

Vorobyov, E. I. 2003, A&A, 407, 913

Wada, K., & Norman, C.A. 2007, ApJ, 660, 276

Wang, B., & Silk, J., 1994, ApJ, 427, 759

Wong, T., & Blitz, L. 2002, ApJ, 569, 157

Zasov, A. V., & Smirnova, A.A. 2005, Ast.L., 31, 160

Ecole Evry Schatzman 2010: Star Formation in the Local Universe
Eds. C. Charbonnel & T. Montmerle
EAS Publications Series, 2011

STAR FORMATION IN SPIRAL ARMS

Bruce G. Elmegreen[1]

Abstract. The origin and types of spiral arms are reviewed with an emphasis on the connections between these arms and star formation. Flocculent spiral arms are most likely the result of transient instabilities in the gas that promote dense cloud formation, star formation, and generate turbulence. Long irregular spiral arms are usually initiated by gravitational instabilities in the stars, with the gas contributing to and following these instabilities, and star formation in the gas. Global spiral arms triggered by global perturbations, such as a galaxy interaction, can be wavemodes with wave reflection in the inner regions. They might grow and dominate the disk for several rotations before degenerating into higher-order modes by non-linear effects. Interstellar gas flows through these global arms, and through the more transient stellar spiral arms as well, where it can reach a high density and low shear, thereby promoting self-gravitational instabilities. The result is the formation of giant spiral arm cloud complexes, in which dense molecular clouds form and turn into stars. The molecular envelops and debris from these clouds appear to survive and drift through the interarm regions for a long time, possibly 100 Myr or more, with lingering spontaneous star formation and triggered star formation in the pieces that are still at high-pressure edges near older HII regions.

1 Introduction

An important feature of many disk galaxies is their spiral structure, which, for the Milky Way, has been connected with star formation since Morgan, Whitford & Code (1953) found concentrations of OB stars in the Sagittarius spiral arm of the Milky Way. This connection suggests that spiral arms trigger star formation, which makes us wonder how such triggering might fit in with the global star formation laws discussed in the previous lecture. The answer is that spiral arms have very little influence on large-scale star formation rates, but they do organize the star

[1] IBM T. J. Watson Research Center, 1101 Kitchawan Road, Yorktown Heights, New York 10598 USA, bge@us.ibm.com

DOI: (will be inserted later)

formation in a galaxy. This is probably because most of the gas that *can* turn molecular, i.e., inside shielded regions at normal interstellar pressure, has already done so in the main disks of galaxies, and because this molecular gas is already forming stars as fast as it can. Star formation in this case may be viewed as saturated (Elmegreen, 2002). Additional cloud collisions in spiral shocks, or new cloud formation in spiral arms, does not add much to the molecular mass and star formation– it only moves it around. This may not be true in the outer parts of galaxies, where the gas is highly atomic. There, dynamical processes such as spiral arms could affect the average star formation rate. There is very little known about outer disks yet, so the influence of outer spiral arms on average star formation rates remains an open question.

In this lecture, we begin with a description of spiral waves and the various theories for them. Then we discuss detailed models for how spiral arms interact with the gas and affect the formation of giant clouds. We also discuss the interarm clouds and the apparent aging and destruction of dense clouds as they move to the next arm.

2 Spiral Waves and Modes

Bertil Lindblad (1962) noticed that $\Omega - \kappa/2$ for angular rotation rate Ω and epicyclic frequency κ was about constant with radius in galaxy disks. He suggested that spirals are fixed patterns with an angular rotation rate $\Omega - \kappa/2$, moving through a disk of stars with a radial variation in the stellar rotation rate Ω. Thus stars and gas move through the spiral pattern. This was the beginning of spiral density wave theory, although it was not quite right yet. Lindblad showed rotation curves for 3 galaxies, Ω versus κ, and a nearly constant $\Omega - \kappa/2$. Rotation curves were difficult measurements at that time, and derivatives in the rotation curves, as in the evaluation of κ, were highly inaccurate.

The main problem with Lindblad's theory was that it had no forcing. Also, $\Omega - \kappa/2$ is not quite constant. Lin & Shu (1964) introduced a more dynamically correct spiral density wave theory. They realized that $\Omega - \kappa/2$ could be forced by the spiral's gravity to a radial-constant value, even if it was not constant from the average rotation curve. Then the stellar orbits could be closed for a wide range of radii at a fixed pattern speed. The angular pattern speed would be slightly different from $\Omega - \kappa/2$, and where it equaled this value, there would be a resonant interaction between the forcing from the spiral and the stellar epicyclic motions. This resonance would absorb wave energy and put it into random stellar motions, causing the wave to stop propagating at this place. This position became known as the inner Lindblad resonance. Another resonance position is where $\Omega + \kappa/2$ equals the spiral pattern speed. This is the outer Lindblad resonance. Other resonances at $\Omega - \kappa/3$ and $\Omega + \kappa/3$, occur as well, limiting the range for three-arm spirals in this case. There are similar limits for 4 arm spirals, etc., and finally the last resonance where Ω itself equals the pattern speed. This is the corotation resonance, where the same stars are always inside the wave crest, following it around at the same angular speed.

The Lin-Shu mechanism works because just inside an arm, spiral gravity pulls a star outward for short time, slowing it down a little as it rises in its epicyclic path. Just outside an arm, spiral gravity pulls the star inward, speeding it up as it falls inward in its epicyclic motion. These slow-downs and speed-ups cause the ends points of each epicycle to advance a little, closing the orbits in a rotating frame with a rate Ω_p such that $\Omega - \kappa/2 < \Omega_p < \Omega + \kappa/2$. The gravitational effect can be seen in the dispersion relation written by Toomre (1969):

$$(\omega - m\Omega[r])^2 = \kappa^2(r) - 2\pi G\Sigma(r)k\mathcal{F}(\chi) \tag{2.1}$$

where ω is the rate of change of the spiral phase in a fixed coordinate system, equal to m times the pattern speed, m is the number of symmetric spiral arms, Σ is the mass column density in the disk, k is the wavenumber, and $\mathcal{F}$ is an integral over stellar motions that depends on $\chi = k^2\sigma_{\rm u}^2/\kappa^2$ for rms radial speed of the stars $\sigma_{\rm u}$. Lindblad's theory did not have the last term on the right, which is from disk gravity. Traveling waves exist for Toomre parameter $Q > 1$, i.e., for disks that are stable to radial perturbations.

Toomre (1969) noted that although the Lin-Shu dispersion relation for spiral waves has a phase velocity equal to the proposed pattern speed, it also has a group velocity which causes the wave crests to move inward, i.e., the spirals wrap up. Thus the "quasi-stationary" spiral density wave theory of Lin, Shu, Roberts, Yuan, and other collaborators at that time, did not work as they originally proposed. Toomre showed that for a flat rotation curve, disk-dominated gravity, and constant stability parameter Q, the Lin-Shu dispersion relation becomes relatively simple,

$$(\omega - m\Omega)/\kappa = \left(m/2^{1/2}\right)[(r/r_{\rm CR}) - 1] \tag{2.2}$$

for radius r and corotation radius $r_{\rm CR}$. In this case, the time derivative of the dimensionless wavenumber increases at a rate equal to half the rate of change in the phase, $\omega/2$. When the wavenumber increases with time, the spirals get closer together, which means they migrate inward. This is a fast migration, almost as fast as purely material arms would wrap up from shear.

Toomre (1969) proposed that spirals are not quasi-stationary, but transient, provoked either by interactions (Toomre & Toomre, 1972) or noise (Toomre & Kalnajs, 1991). Kormendy & Norman (1979) noted that "grand design" spirals are either in barred galaxies, in the rising parts of rotation curves (where $\Omega - \kappa/2 \sim 0$) or in interacting galaxies. This would be consistent with Toomre's picture. Toomre (1981) identified the cause of transient spirals as "swing amplified instabilities." Many groups have studied these instabilities numerically (e.g., Fuchs et al., 2005).

The quest for a theory of quasi-stationary spiral structure was not over, though. Mark (1974), Lau et al. (1976), and Bertin et al. (1989) proposed a "modal theory" in which inward-moving waves reflect or refract off of a bulge or bar and come back out as leading (WASER2; reflection) or trailing (WASER1; refraction) spiral arms. When they reach the corotation resonance moving outward, they amplify. Part of the wave then turns around to come back in and another part of the wave keeps going outward. The result is a standing wave pattern, amplified from initial

disk noise at corotation and forming a long-lived grand-design spiral. The corotation radius is where the outward-moving wave meets the inward-moving wave on the opposite side of the galaxy for a two-arm spiral. If the outward moving wave is leading, then at the meeting place, the swing amplifier can transform this leading wave into a strong trailing wave. For example, an inward moving wave starting at corotation in one arm of a two-arm spiral can reflect off of a bulge and move back out as a leading wave until it meets the other arm at the same radius where it started. It amplifies as it is converted into a trailing arm, adds to the original trailing arm, and then a stronger trailing arm comes in again. Trailing waves that start at different radii will not reflect and meet the opposite arm at the same radius, and so will not add to the original wave after amplification. Thus, out of all the disk noise and small spirals that they initiate, only the spiral with the ability to amplify reflected or refracted waves and reinforce itself will grow. This defines the corotation radius. Bertin et al. (1989) described this process in detail.

Spiral wave modes could exhibit an interference pattern between the inward and outward moving waves. Interference acts to modulate the amplitudes of the main arms or it may introduce slight phase shifts in the main arms. Such modulation is present in the model solutions shown by Bertin et al. (1989). Elmegreen et al. (1992) reported such interference patterns, but a more modern analysis is needed.

The various theories of spiral wave formation may be reduced to four basic types: random and localized swing-amplified spirals that are primarily in the gas (because the stellar disk is somewhat stable); random and localized swing-amplified spirals that are in the stars and the gas together; transient global waves that are in the stars and gas, and standing wavemodes that are in the stars and gas. The first type produces flocculent spiral arms and a smooth underlying stellar disk (e.g., NGC 5055), the second type produces multiple stellar and gaseous arms (e.g., NGC 3184), the third type produces long spiral arms in the stars and gas (e.g., NGC 628), and the fourth type produces strong two-arm spirals in the stars and gas, usually in response to some global perturbation like a galaxy interaction (e.g., M51, M81). Aside from M81, these galaxy examples were chosen from the THINGS survey (Walter et al., 2008).

A spiral wavemode may be compared to the pure-tone ringing of a bell after some multi-frequency impact disturbs it (e.g., it is hit by a hammer or bowed by a violin string). Random swing-amplified spirals have been called spiral chaos. They are the primary response to gravitational instabilities in the stars and gas and therefore have a strong connection with star formation and the origin of interstellar turbulence in the absence of global wavemodes (e.g., Thomasson et al., 1992; Bournaud et al., 2010). Global spiral waves or wavemodes also have a connection with star formation because of the way they force the gas into a dense molecular phase in the dust lanes (which are shock fronts) and organize it to follow the underlying stellar spiral.

3 Motions in Spiral Arms

Because of the forcing from gravity, spiral arms induce a reverse shear in the stellar rotation, slowing down the stars on the inner parts and speeding up the stars on the outer parts of each arm Roberts (1969). This reverse often cancels the normal shear from average orbital motions, and makes an arm that has very little internal shear. The arm forcing from gravity also pulls everything in the arm toward the center of the arm, i.e., in a convergent manner, which is opposite to the tidal force from the surrounding galaxy. Thus spiral arms also have reduced galactic tidal forces (Elmegreen, 1992). These conditions are good for the formation of large cloud complexes, which are only weakly bound at the start. Giant clouds that form by gravitational instabilities in spiral arms do not immediately shear out into little spirals, and this allows them to grow. When they emerge from the arm, the shear rate and tidal disruption rate increase a lot, and the low-density parts of the clouds can come apart. They can also form feathers and spurs. Such feathering is commonly seen (La Vigne et al., 2006). Feathers occur primarily in grand design (2-arm) galaxies with prominent dust lanes. The feathers are closer where gas density is highest, as expected for gravitational instabilities. Their separation is $5-10$ Jeans lengths in the dust lane (La Vigne et al., 2006).

The peculiar motions from spiral arm gravity and Coriolis forces cause the gas and stars to stream along the spiral arms when they are in the arms, and to expand away from the arms when they are between the arms. Streaming motion of the gas can be very strong, perhaps 50 km s^{-1} or more, as in M51 (Shetty et al., 2007). Radial streaming changes sign at corotation and the observation of this allows one to locate the corotation resonance radius (e.g., Elmegreen et al., 1998). Streaming motions also allow one to measure the timing of the star formation response to the spiral arm (Tamburro et al., 2008). The streaming pattern for gas tends to be inward inside the main parts of the arms inside the corotation radius, and outward in the interarms inside corotation. This pattern of radial motions relative to the arms reverses outside of corotation. Thus the gas and star formation in outer disk spirals, as viewed, for example, by GALEX, should be streaming with positive galacto-centric radial velocities, whereas the gas and star formation in inner disk spirals should be streaming with negative galacto-centric radial velocities. Shetty et al. (2007) found a net radial inward streaming flux for the inner part of M51, including both the arms and the interarms. They suggested that this meant a non-steady spiral pattern.

4 Magnetic Fields in Spiral Arms

The magnetic fields of spiral galaxies have been extensively observed, particular by Rainer Beck and collaborators (e.g., Braun et al., 2010) using Faraday rotation. In NGC 6946 (Beck, 2007), the field structure is uniform in the interarm regions, probably from the combing action of shear with little disruption from star formation. It is more chaotic in the arms, and even weaker on average in the arms than the interarms because of the strong random component in the arms. The

total field strength in the arms should be higher than in the interarms because of compression from the spirals, but this higher field strength might not be seen with rotation measures if the field direction fluctuates on small scales.

Gravitational instabilities in spiral arm gas are enhanced by the lack of shear and the magnetic field (Elmegreen, 1987), which tends to run parallel to the arms in the direction of the unstable flow. This field removes angular momentum from a growing condensation, as mentioned in Lecture 1. Kim & Ostriker (2001) have dubbed this the Magneto-Jeans instability, and modeled it numerically. Gas collapses along spiral arms into giant cloud complexes, aided by the parallel magnetic field. The dense gas then emerges downstream from the arms as interarm feathers.

5 Gravitational Instabilities in Spiral Arms

Gas rich galaxies with weak stellar spirals have more interarm gas and star formation than galaxies with strong stellar spirals. In weak-arm spiral galaxies, local swing-amplified instabilities in the gas become prominent and these can occur almost anywhere. In galaxies with strong, global stellar waves, the magneto-Jeans instability forms giant cloud complexes primarily in the spiral arms, where the density is high and the shear is low.

Figure 1 shows a Hubble Space Telescope image of the galaxy NGC 4414, which has numerous patches of star formation in the midst of a faint 2-arm structure. This is an example of the first type mentioned in the previous paragraph. Figure 2 shows an HST image of M51, a strong two-arm spiral with little star formation between the stellar arms. This is an example of the second type.

Stellar spirals define two scales, $2\pi G\Sigma/\kappa^2$, which is the "Toomre length"

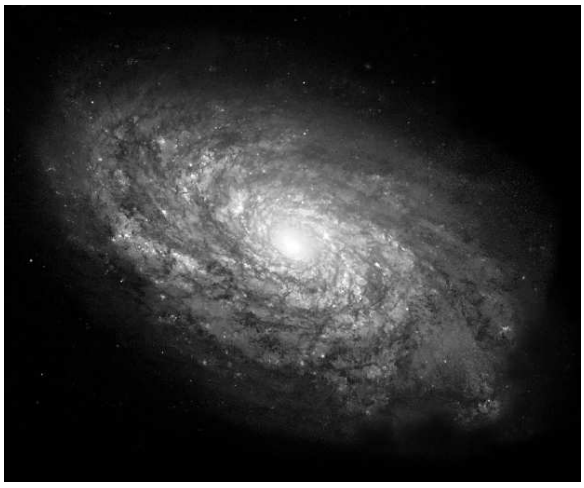

Fig. 1. Hubble Space Telescope image of NGC 4414, from multiple passbands.

(Toomre, 1964) separating the spirals, and $2\sigma^2/G\Sigma$, which is the Jeans length separating the condensations in the spirals. The Jeans length is about three times the arm width and physically smaller inside the dense dust lanes. The beads on a string seen in spiral arms are giant star complexes. Each has a feather or spur of dust from a spiral wave flow downstream. This is clearly visible in the HST image of M51, shown in Figure 2. In the interarm regions of M51, young stars are still in star complexes that are aging. Lingering star formation and triggered star formation occur in the interarm fields of cloudy debris. Further downstream, the cloud envelopes are more diffuse but there is still a little star formation in some of them (Fig. 3). The molecular envelopes of GMCs must be long-lived to survive as far as they do downstream from the arms, ~ 100 Myr or more. This seems to require magnetic support in the cloud envelopes (Elmegreen, 2007). Further downstream, almost at the next spiral arm, the cloudy debris from the previous arm has little associated star formation. There appears to be a lot of diffuse molecular gas indicated by these interarm dust features. They coagulate into a dust lane when they reach the next arm.

At a very basic level, a gravitational instability in a spiral arm, or in a spiral arm dust lane (Elmegreen, 1979) can be viewed as an instability in a cylinder.

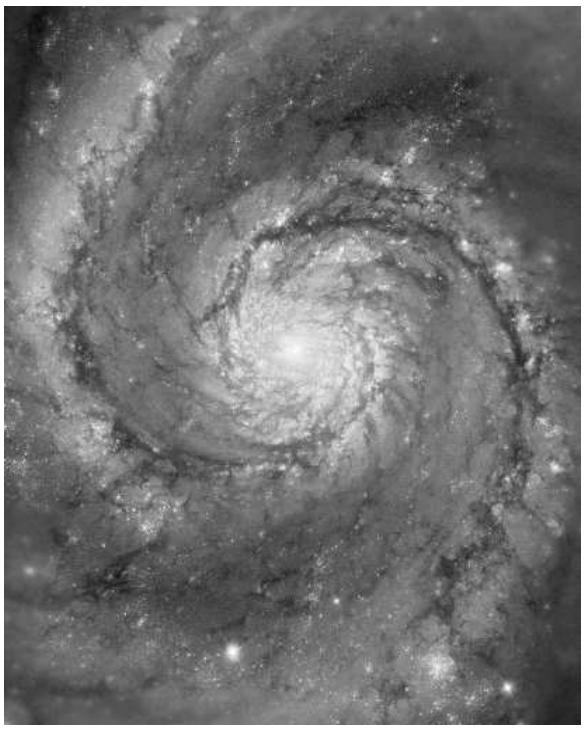

Fig. 2. Hubble Space Telescope image of NGC 5194, from multiple passbands.

Such instabilities occur when

$$\pi G\mu/\sigma^2 \geq 1 \tag{5.1}$$

where μ is the mass per unit length in the cylinder and σ is the velocity dispersion. The fastest growing mode has a wavelength of about 3 times the cylinder width (Elmegreen & Elmegreen, 1983).

There is also enhanced star formation at the end of some strong bars. This is most likely a crowding effect from the gas that turns a corner there in its orbit relative to the bar (Lord & Kenny, 1991). The inner, nearly straight, dust lanes in many bars do not contain much star formation and look non-self gravitating. This is probably because of high shear and radial tidal forces. Inside this dustlane, in the center of the bar, there is often a ring close to the inner Lindblad resonance (Buta & Combes, 1996). This ring also has two characteristic scales, the thickness in the radial direction and the Jeans length. ILR rings develop major

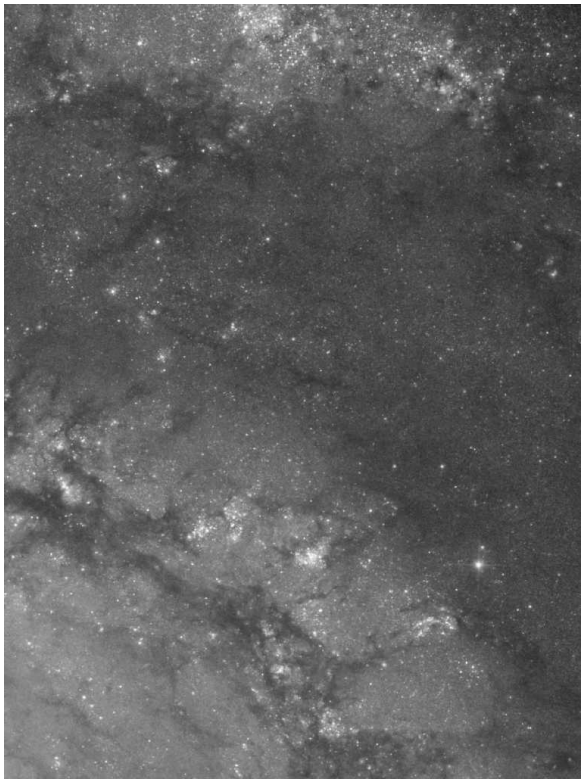

Fig. 3. Enlargement of the Western interarm region of M51, from the Hubble Space Telescope image. Dark dust clouds with small amounts of star formation, or no evident star formation, are seen. Some are at the edges of old OB associations and may contain triggered star formation.

sites of star formation, or "hot-spots" along them, with a separation of around the Jeans length, probably because of local gravitational instabilities in the gas (e.g., Elmegreen, 1994).

6 Star Formation in Spiral Arms

What is the relationship between HI, CO and star formation in spiral arms? The gas is generally compressed more than the stars in a spiral density wave or swing-amplified transient spiral, and if star formation follows the gas, then the blue light from star formation will be enhanced more than the yellow and red light from old stars. This makes the spirals arms blue. The Bigiel et al. (2008) and Leroy et al. (2008) correlation between SF rate and CO, which is a very tight correlation, implies that there is little difference in the rate per unit CO molecule for gas in strong-arm galaxies compared to gas in weak-arm galaxies.

The morphology of gas in the arms tells something about the star formation process. Grabelsky et al. (1987) showed that most of the CO clouds in the Carina arm of the Milky Way are clustered together in the cores of 10^7 $M_\odot$ HI clouds. Elmegreen & Elmegreen (1987) found the same for the Sagittarius spiral arm. Lada et al. (1988) observed a similar HI envelope-CO core structure in a piece of a spiral arm in M31. Engargiola et al. (2003) showed a complete map of M33 with numerous CO clouds in the cores of giant HI clouds. The presence of giant HI clouds in spiral arms has been known for a long time (e.g., for the Milky Way: McGee & Milton 1964; for NGC 6946: Boulanger & Viallefond 1992). Now it looks like most dense molecular clouds are in the cores of giant spiral arm HI clouds, or if the gas is highly molecular at that radius in the disk, in the cores of giant clouds that are also highly molecular. This means that GMCs form by condensation inside even larger, lower-density clouds. The large HI/CO clouds, in turn, probably form by gravitational instabilities in the spiral arm gas, particularly in the dust lanes where the spiral shock brings the gas to a high density. Recall from Lecture 1 that the largest unstable clouds have the Jeans mass in a galaxy disk, given the observed turbulent speed and column density (i.e., $M \sim \sigma^4/G^2\Sigma_{\rm gas} \sim 10^7\ M_\odot$).

In the Milky Way and M33, giant spiral arm clouds are mostly atomic, but in M51, they are mostly molecular (Ranf & Kulkarni, 1990). This difference is presumably because the arms in M51 are much stronger than the arms in the Milky Way and M33, and the gas is denser overall in M51 as well. Thus, the pressure is higher in M51, particularly in the arms, and the gas is more highly molecular there and everywhere else in the inner disk. The physical process of giant cloud formation should be the same in all three cases, however.

Gravitational instabilities also seem to initiate cloud and star formation on the scale of whole galaxies. This process is clear in many regions, such as Stephans quintet (Mendes de Oliveira et al., 2004), NGC 4650 (Karataeva et al., 2004), and in the tidal arcs of NGC 5291 (Bournaud et al. 2007), where there are massive condensations in tidal features.

Dobbs & Pringle (2009) studied gravitationally bound clouds in an SPH simulation. In the spiral arms, large regions formed by gravitational instabilities where

gravity balanced thermal, turbulent and magnetic energies. When they used a star formation rate equal to 5% of the bound gas column density divided by the dynamical time, plotted versus the total gas column density, they reproduced the Kennicutt (1998) and Bigiel et al. (2008) star formation laws over the range of overlap. They noted that the star formation law is linear with column density because the dynamical time inside each bound cloud is the same, i.e., they all have the same density. They answered the long-time question of whether density waves trigger star formation (Elmegreen & Elmegreen, 1986) by saying, no, there is no correlation between the average column density of star formation and the spiral arm potential depth. The reason is that stronger spiral waves make clouds with higher velocity dispersions and they are harder to bind into gravitating cloud complexes. The fraction of the bound gas in spiral arms increases with the spiral strength, but not the star formation rate.

Observations of spiral arm star formation and gas distributions also suggest there is little triggering (Foyle et al., 2010). The primary effect of the spiral is to concentrate the gas in the arms without significantly changing the star formation rate per unit gas.

7 Summary

Spirals can, in principle, be of 4 types: (1) Transient gravitational instabilities in the gas, causing "flocculent spirals," with too much stability in the stellar disk to give prominent stellar spiral waves. (2) Transient gravitational instabilities in the stars, with the gas adding force and following the stars. The gas and stars move through these transient spirals a little, but not around from arm to arm in a full circle as in idealized global stellar modes and waves. (3) Global stellar waves that are non-steady with a pattern speed that varies with radius and whose patterns wrap up toward the center over time. Stars and gas move through these spirals. (4) Global stellar wave modes that are "standing waves," with a uniform pattern speed between the Lindblad resonances. Gas and stars move through these standing waves with corotation approximately at mid-radius in the spiral.

Young stars concentrate in spiral arms because the gas concentrates there. Spiral arms are dense and promote more gravitational instabilities and cloud collisions than the interarm regions, triggering molecular cloud formation and conglomeration in the arms. The star formation rate per unit area is high in the arms as a result. This excess star formation rate is mostly in proportion to the extra molecular gas column density there, without a significant change in the star formation rate per unit molecular gas mass. The total galactic star formation rate in the main disk is not significantly enhanced by the presence of spiral arms. That is like saying the gas would have formed the same abundance of molecular clouds even without the arms. Outer disks may be different. They may have an excess of total star formation if there are spiral arms there, but this excess has not been observed yet. The difference between inner disks and outer disks is that inner disks are highly molecular and star formation in the gas is virtually saturated. Outer disks are mostly atomic and without star formation, so triggering a higher rate of star

formation might be possible with dynamical disturbances.

References

Beck, R. 2007, A&A, 470, 539

Bertin, G., Lin, C. C., Lowe, S. A., & Thurstans, R. P. 1989, ApJ, 338, 104

Bigiel, F., Leroy, A., Walter, F., Brinks, E., de Blok, W. J. G., Madore, B., & Thornley, M. D. 2008, AJ, 136, 2846

Boulanger, F., & Viallefond, F. 1992, A&A, 266, 37

Bournaud, F., Duc, P.-A., Brinks, E., Boquien, M., Amram, P., Lisenfeld, U., Koribalski, B.S., Walter, F., & Charmandaris, V. 2007, Sci., 316, 1166

Bournaud, F., Elmegreen, B.G., Teyssier, R., Block, D.L., & Puerari, I. 2010, MNRAS, in press, arXiv:1007.2566.

Braun, R., Heald, G., & Beck, R. 2010, A&A, 514, 42

Buta, R., & Combes, F. 1996, Fund.Cosmic Phys., 17, 95

Dobbs, C. L., & Pringle, J. E. 2009, MNRAS, 396, 1579

Elmegreen, B.G. 1979, ApJ, 231, 372

Elmegreen, B.G. 1987, ApJ, 312, 626

Elmegreen, B.G. 1992, in SAAS FEE Lectures, "The Galactic Interstellar Medium," with W.B. Burton and R. Genzel, ed. D. Pfenniger and P. Bartholdi, Berlin: Springer, p. 157

Elmegreen, B.G. 1994, ApJL, 425, 73

Elmegreen, B.G. 2002, ApJ, 577, 206

Elmegreen, B.G. 2007, ApJ, 668, 1064

Elmegreen, B.G., & Elmegreen, D.M. 1983, MNRAS, 203, 31

Elmegreen, B.G., & Elmegreen, D.M. 1986, ApJ, 311, 554

Elmegreen, B.G., & Elmegreen, D.M. 1987, ApJ, 320, 182

Elmegreen, B.G., Elmegreen, D.M., & Montenegro, L. 1992, ApJS, 79, 37

Elmegreen, B.G., Wilcots, E., & Pisano, D. J. 1998, ApJ, 494, L37

Engargiola, G., Plambeck, R. L., Rosolowsky, E., & Blitz, L. 2003, ApJS, 149, 343

Foyle, K. Rix, H.-W., Walter, F., & Leroy, A. 2010, arXiv:1010.0678

Fuchs, B., Dettbarn, C., & Tsuchiya, T. 2005, A&A, 444, 1

Grabelsky, D. A., Cohen, R. S., Bronfman, L., Thaddeus, P., & May, J. 1987, ApJ, 315, 122

Karataeva, G. M., Drozdovsky, I. O., Hagen-Thorn, V. A., Yakovleva, V. A., Tikhonov, N. A., & Galazutdinova, O. A. 2004, AJ, 127, 789

Kennicutt, R.C., Jr. 1998, ApJ, 498, 541

Kim, W.-T., & Ostriker, E.C. 2001, ApJ, 559, 70

Kormendy, J., & Norman, C. A. 1979, ApJ, 233, 539

Lada, C.J., Margulis, M., Sofue, Y., Nakai, N., & Handa, T. 1988, ApJ, 328, 143

Lau, Y.Y., Lin, C.C. & Mark, J.W.-K. 1976, Pub. National. Acad. Sciences, 73, 1379

La Vigne, M.A., Vogel, S.N., & Ostriker, E.C. 2006, ApJ, 650, 818

Leroy, A.K., Walter, F., Brinks, E., Bigiel, F., de Blok, W. J. G., Madore, B., & Thornley, M. D. 2008, AJ, 136, 2782

Lin, C. C., Shu, F.H. 1964, ApJ, 140, 646

Lindblad, B., 1962, IAUS, 15, 146

Lord, S.D., & Kenney, J.D.P. 1991, ApJ, 381, 130

Mark, J.W.-K. 1974, ApJ, 193, 539

McGee, R. X., & Milton, J.A. 1964, Aust.J.Phys., 17, 128

Mendes de Oliveira, C., Cypriano, E. S., Sodré, L., Jr., & Balkowski, C. 2004, ApJ, 605, 17

Morgan, W. W., Whitford, A. E., & Code, A. D. 1953, ApJ, 118, 318

Rand, R.J., & Kulkarni, S.R. 1990, ApJ, 349, L43

Roberts, W. W. 1969, ApJ, 158, 123

Shetty, R., Vogel, S.N., Ostriker, E.C., & Teuben, P.J. 2007, ApJ, 665, 1138

Tamburro, D., Rix, H.-W., Walter, F., Brinks, E., de Blok, W. J. G., Kennicutt, R. C., & Mac Low, M.-M. 2008, AJ, 136, 2872

Thomasson, M., Donner, K.H., & Elmegreen, B.G. 1992, A&A, 250, 316

Toomre, A. 1964, ApJ, 139, 1217

Toomre, A. 1969, ApJ, 158, 899

Toomre, A. 1981, in "The structure and evolution of normal galaxies," Cambridge: Cambridge University Press, p. 111.

Toomre, A., & Toomre, J. 1972, ApJ, 178, 623

Toomre, A., & Kalnajs, A. J. 1991, in Dynamics of Disc Galaxies: Varberg Castle Sweden, p. 341

Walter, F., Brinks, E., de Blok, W.J.G., Bigiel, F., Kennicutt, R.C., Jr., Thornley, M.D., & Leroy, A. 2008, AJ, 136, 2563

Ecole Evry Schatzman 2010: Star Formation in the Local Universe
Eds. C. Charbonnel & T. Montmerle
EAS Publications Series, 2011

STAR FORMATION PATTERNS AND HIERARCHIES

Bruce G. Elmegreen[1]

Abstract. Star formation occurs in hierarchical patterns in both space and time. Galaxies form large regions on the scale of the interstellar Jeans length and these large regions apparently fragment into giant molecular clouds and cloud cores in a sequence of decreasing size and increasing density. Young stars follow this pattern, producing star complexes on the largest scales, OB associations on smaller scales, and so on down to star clusters and individual stars. Inside each scale and during the lifetime of the cloud on that scale, smaller regions come and go in a hierarchy of time. As a result, cluster positions are correlated with power law functions, and so are their ages. At the lowest level in the hierarchy, clusters are observed to form in pairs. For any hierarchy like this, the efficiency is automatically highest in the densest regions. This high efficiency promotes bound cluster formation. Also for any hierarchy, the mass function of the components is a power law with a slope of around -2, as observed for clusters.

1 Introduction

Local Open Clusters in the compilation by Piskunov et al. (2006) seem at first to have a random distribution in the galactic plane, with the local spiral arms barely visible and no obvious age gradients or patterns. They have been known to be grouped into star complexes (Efremov, 1995) and moving groups (Eggen, 1989) for a long time, but there has been little other patterning recognized. Now this is beginning to change. The groupings and complexes are better mapped using new velocity and distance information. Piskunov et al. (2006) and Kharchenko et al. (2005) catalogued "Open Cluster Complexes," in which many clusters have similar positions, velocities and ages inside each complex. For example, one is in the Hyades region and another is in Perseus-Auriga. Perseus-Auriga surrounds the Sun and lies in the galactic plane over a region 1 kpc in size with a log(age) between 8.3 and 8.6, in years. Gould's Belt is another Open Cluster Complex. It

[1] IBM T. J. Watson Research Center, 1101 Kitchawan Road, Yorktown Heights, New York 10598 USA, bge@us.ibm.com

DOI: (will be inserted later)

has a log age less than 7.9 and lies in a thin plane tilted to the main galactic disk by an angle of 20° surrounding the Sun.

de la Fuente Marcos & de la Fuente Marcos (2008) identified five Open Cluster Complexes from the positions and velocities of clusters within 2.5 kpc of Sun. These are: Scutum-Sagittarius at a galactic longitude of $l = 12°$ and a distance of 1300 pc, Cygnus at $l = 75°$ and 1400 pc, Cassiopeia-Perseus at $l = 132°$ and 2000 pc, Orion at $l = 200°$ and 500 pc, and Centaurus-Carina at $l = 295°$ and 2000 pc. These authors suggest that Open Cluster Complexes are fragments from common gas clouds. Within their limiting distance of 2.5 kpc, the total gas mass in the Milky Way is $\sim 5 \times 10^7\ M_\odot$, considering a disk thickness of 300 pc and an average density of 1 cm^{-3}. This means that each of the 5 giant gas clouds that made these Open Cluster Complexes had a mass of $\sim 10^7\ M_\odot$. This is the Jeans mass in the galactic disk ($\sim \sigma^4/[G^2\Sigma_{\rm gas}]$ for dispersion σ and mass column density $\Sigma_{\rm gas}$), as discussed in Lecture 1. Open Cluster Complexes could be the remnants of star formation in giant clouds formed by gravitational instabilities in the Milky Way gas layer.

Elias, Alfaro & Cabrera-caño (2009) studied Gould's Belt using the Catalogue of Open Cluster Data (Kharchenko et al., 2005). They found an interesting correlation that the cluster fraction is large for the Orion OB association region and small for the Sco-Cen association. The cluster fraction is the ratio of the stellar mass that forms in bound clusters to the total stellar mass that forms at the same time. The rest of the stars form in unbound groups and associations. There is a gradient in the young cluster (age < 10 Myr) fraction of star formation and in the cluster density over the 700 pc distance separating these two associations. This suggests that star formation prefers clusters when the pressure is high, as in Orion, which is a more active region than Sco-Cen. High pressure could be a factor in bound cluster formation if high-pressure cores are more difficult to disrupt and their star formation efficiencies end up higher when star formation stops. High pressure also corresponds to a broader density probability distribution function, and so a higher mass fraction of gas exceeding the critical efficiency for bound cluster formation (Sect. 7).

This lecture reviews interstellar and stellar hierarchical structure, which gives patterns in the positions and ages of young stars and clusters. Related to this is the formation of the bound clusters themselves, and the cluster mass function. A more complete review of this topic is in Elmegreen (2010).

2 Galactic Scale

The hierarchy of star formation begins on the scale of Jeans-mass cloud complexes. Giant molecular clouds (GMCs) form by molecular line shielding and condensation inside these giant clouds, and star complexes build up from the combined star formation (Elmegreen & Elmegreen, 1983). Each GMC makes a single OB association at any one time. Hierarchical structure has been known to be important in star-forming regions for a long time (e.g., Larson, 1981; Feitzinger & Galinski, 1987). Early reviews of large-scale hierarchical structure are in Scalo (1985, 1990).

Interstellar hierarchies have also been thought to have a possible role in the stellar initial mass function (e.g., Larson, 1973, 1982, 1991).

The nearby galaxy M33 has a clear pattern of giant HI clouds, with masses of $10^6 - 10^7\ M_\odot$, containing most of the GMCs and CO emission (Engargiola et al., 2003). Giant star complexes occur in these regions (Ivanov, 2005), often extending beyond the HI clouds because of stellar drift. The high-definition image of M51 made by the ACS camera on the Hubble Space Telescope shows exquisite examples of stellar clustering on a wide variety of scales, with similar patterns of clustering for dust clouds, which are the GMCs (Fig. 1). Clearly present are giant clouds (1 kpc large with $M \sim 10^7\ M_\odot$) that are condensations in spiral arm dust lanes, star formation inside these clouds with no noticeable time delay after the spiral shock, and scattered star formation downstream. The downstream activity has the form of lingering star formation in cloud pieces that come from the disassembly of spiral arm clouds, in addition to triggered star formation in shells and comet-shaped clouds that are also made from the debris of spiral arm clouds (see Lectures 2 and 4).

Star clusters in M51 observed with HST have been studied by Scheepmaker et al. (2009). The overall distribution of clusters in the M51 disk shows no obvious correlations or structures, aside from spiral arms. But autocorrelation functions for three separate age bins show that the youngest sample is well correlated: it is hierarchical with a fractal dimension of ~ 1.6. This means that there are clusters inside cluster pairs and triplets, that are inside clusters complexes and so on, up to ~ 1 kpc. Clusters in the Antennae galaxy are also auto-correlated out to ~ 1 kpc scales (Zhang, Fall, & Whitmore, 2001).

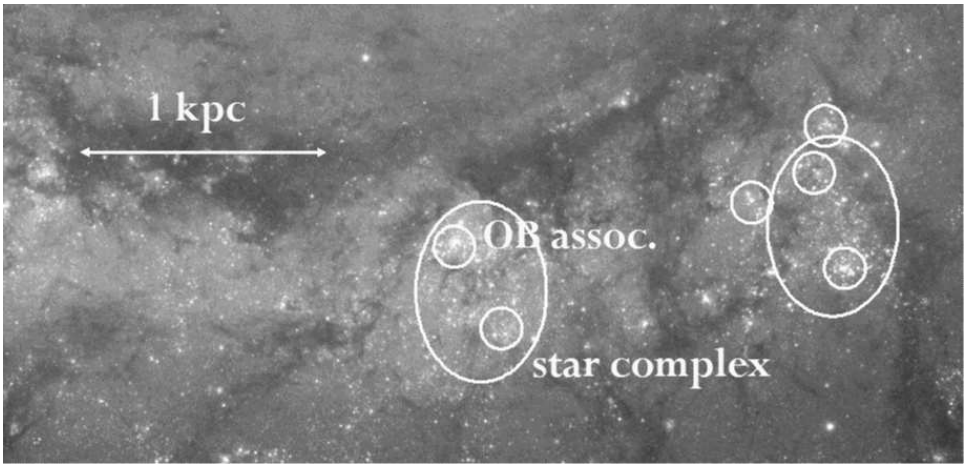

Fig. 1. The Southern part of the inner spiral arm of M51, showing star formation on a variety of scales, with OB associations inside star complexes and gas structures all around. The dust lane is broken up into giant cloud complexes that contain $10^7\ M_\odot$.

Sánchez & Alfaro (2008) surveyed the positions of HII regions in several galaxies. They found that the fractal dimension, D_c, of the distribution of HII regions decreases with increasing HII region brightness. For NGC 6946, $D_c = 1.64$ for high-brightness HII regions, $D_c = 1.82$ for medium-brightness, and $D_c = 1.79$ for low-brightness. They also found that among galaxies with more than 200 HII regions, the fractal dimension decreases slightly with decreasing galaxy brightness.

The fractal dimension is the ratio of the log of the number N of substructures in a region to the log of the relative size S of these substructures. If we imagine a square divided into 3×3 subsquares, which are each divided into 3×3 more subsquares, and so on, then the size ratio is $S = 3$ for each level. If 6 of these subsquares actually contain an object like an HII region (so the angular filling factor is 6/9), then $N = 6$ and the fractal dimension is $\log 6/\log 3 = 1.63$. If all 9 regions contain substructure, then the fractal dimension would be $\log 9/\log 3 = 2$, which is the physical dimension of the region, viewed in a 2-dimensional projection on the sky. Thus a low fractal dimension means a small filling factor for each substructure in a hierarchy of substructures. If the brightest HII regions have the smallest fractal dimension in a galaxy, then this means that the brightest HII regions are more clustered together into a smaller fraction of the projected area. This greater clustering is also evident from maps of the HII region positions as a function of brightness (Sánchez & Alfaro, 2008). The brightest HII regions tend to be clustered tightly around the spiral arms. Similarly, fainter galaxies have more tightly clustered HII regions than brighter galaxies.

The size distributions of star-forming regions can also be found by box-counting. Elmegreen et al. (2006) blurred an HST/ACS image of the galaxy NGC 628 in successive stages and counted all of the optical sources at each stage with the software package *SExtractor*. The cumulative size distribution of structures, which are mostly star-forming regions, was a power law with power 2.5 for all available passbands, B, V, and I, i.e., $n(> R)dR \propto R^{-2.5}dR$ for size R. The Hα band had a slightly shallower power. They compared this distribution with the distribution of structures in a projected 3D model galaxy made as a fractal Brownian motion density field. They got good agreement when the power spectrum for the model equalled the 3D power spectrum of Kolmogorov turbulence, which has a slope of 3.66. Other power spectra gave either too little clumpiness of the structures (lower $n[> R]$ slope) or too much clumpiness (higher slope).

Azimuthal intensity profiles of optical light from galaxies have power-law power spectra like turbulence too. Elmegreen et al. (2003) showed that young stars and dust clouds in NGC 5055 and M81 have the same scale-free distribution as HI gas in the LMC (Elmegreen et al., 2001), both of which have a Kolmogorov power spectrum of structure. For azimuthal scans, the power spectrum slope was $\sim -5/3$ in all of these cases. Block et al. (2009) made power spectra of Spitzer images of galaxies. They included M33, which is patchy at 8μm where PAH emission dominates, and relatively smooth at 3.6μm and 4.5μm where the old stellar structure dominates. The power spectra showed this difference too: the slopes were the same as those of pure noise power spectra for the stellar images, and about the same as Kolmogorov turbulence for the PAH images. The grand-

design galaxy M81 had the same pattern. Block et al. also reconstructed images of the galaxies over the range of Fourier components that gave the power-law power spectrum. These images highlight the resolved hierarchical parts of the galaxies. These parts are primarily star complexes and young stellar streams.

The central regions of some galaxies show highly structured dust clouds in HST images. The central disk in the ACS image of M51 shows this, for example. In the central regions of these galaxies, there are large shear rates, strong tidal-forces, sub-threshold column densities, strong radiation fields, and lots of holes and filaments in the dust. The origin of the holes is not known, although it is probably a combination of radiation pressure, stellar winds, and turbulence. Irregular dust in the center of NGC 4736 was studied by Elmegreen et al. (2002) using two techniques. One used unsharp mask images, which are differences between two smoothed images made with different Gaussian smoothing functions. Unsharp masked images show structure within the range of scales given by the smoothing functions. They also made power spectra of azimuthal scans. The power spectra were found to be power laws with a slope of around $-5/3$, the same as the slope for HI in the LMC and optical emission in NGC 5055 and M81. A possible explanation for the power-law dust structure in galactic nuclei is that this is a network of turbulent acoustic waves that have steepened into shocks as they move toward the center (Montengero et al., 1999).

Block et al. (2010) made power spectra of the Spitzer images of the Large Magellanic Cloud at 160μ, 70μ, and 24μ (see Figure 2). Again the power spectra are power laws, but now the power laws have breaks in the middle, as found previously in HI images of the LMC (Elmegreen et al., 2001). These breaks appear to occur at a wavenumber that is comparable to the inverse of the disk line-of-sight thickness. On scales smaller than the break, the turbulence is 3D and has the steep power spectrum expected for 3D, and on larger scales the turbulence is 2D and has the expected shallower spectrum. The LMC is close enough that each part of the power spectrum spans nearly two orders of magnitude in scale. The slopes get shallower as the wavelength of the observation decreases, so there is more small-scale structure in the hotter dust emission.

Power-law power spectra in HI emission from several other galaxies were studied by Dutta and collaborators. Dutta et al. (2008) obtained a power spectrum slope of -1.7 covering a factor of 10 in scale for NGC 628. Dutta et al. (2009a) found two slopes in NGC 1058 with a steepening from -1 to -2.5 at an extrapolated disk thickness of 490 pc (although their spatial resolution did not resolve this length). Hα and HI power spectra of dwarf galaxies showed single power laws (Willett et al., 2005; Begum et al., 2006; Dutta et al., 2009b), as did the HI emission (Stanimirovic et al., 1999) and dust emission (Stanimirovic et al., 2000) of the Small Magellanic Cloud. The SMC has an interesting contrast to the LMC, both of which are close enough to make a power spectrum over a wide range of spatial scales. The LMC has a two component power spectrum, but the SMC has only a single power-law slope. The difference could be because the line-of-sight depth is about as long as the transverse size for the SMC, while the line-of-sight depth is much smaller than the transverse size for the LMC.

3 Time-Space Correlations

In addition to being correlated in space, clusters are also correlated in time. Efremov & Elmegreen (1998) found that the age difference between clusters in the LMC increases with the spatial separation as a power-law, age $\propto$ separation$^{1/2}$. Elmegreen & Efremov (1996) found the same age-separation correlation for Cepheid variables in the LMC. de la Fuente Marcos & de la Fuente Marcos (2009a) showed that this correlation also applies to clusters in the solar neighborhood. In both cases, the correlation is strongest for young clusters with a separation less than $\sim$ 1 kpc, and it goes away for older clusters. Presumably the young clusters follow the correlated structure that the gas had when the clusters formed. Clusters form faster in regions with higher densities out to a kpc or so, which is probably the ISM Jeans length. This means that small star-forming regions (e.g., cluster cores) come and go during the life of a larger star-forming region (an OB association), and then the larger regions come and go during the life of an even larger region (a star complex). Eventually, the clusters, associations and complexes disperse when they age, taking more random positions after $\sim$ 100 Myr. The correlation is about the same as the size-linewidth relation for molecular clouds (Larson, 1981),

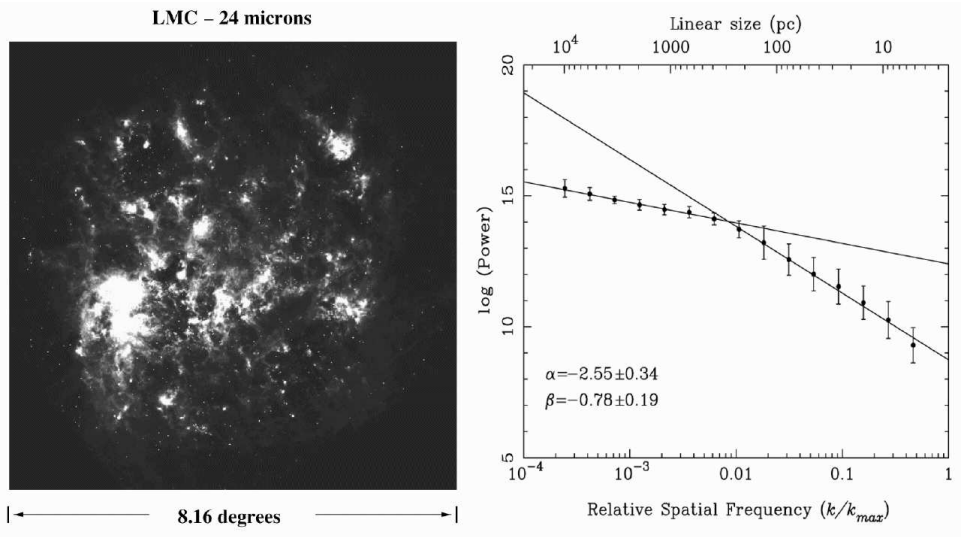

Fig. 2. (Left) An image of the LMC at 24μm from the Spitzer Space Telescope. (Right) The 2D power spectrum of this image, showing two power-law regions. The region with high slope at large spatial frequency k is presumably 3D turbulence inside the thickness of the disk, and the region with low slope at small k is presumably from 2D turbulence and other motions on larger scales. The break in the slope defines the scale of the disk thickness (from Block et al., 2010).

considering that the ratio of the size to the linewidth is a timescale.

Correlated star formation implies that some clusters should form in pairs. Cluster pairs were discovered in the LMC by Bhatia & Hatzidimitriou (1988) and in the SMC by Hatzidimitriou & Bhatia (1990). An example is the pair NGC 3293 and NGC 3324 near eta Carinae. de la Fuente Marcos & de la Fuente Marcos (2009b) studied these and other pairs. For NGC 3292/3324, the clusters are apparently weakly interacting and the age difference is 4.7 My. NGC 659 and NGC 663 are also weakly interacting and the age difference is 19.1 My. Dieball et al. (2002) determined the distribution function of the number of cluster members per cluster group in the LMC. They found a statistical excess of clusters in pairs compared to the expectation from random groupings.

4 Correlated Star Positions

Individual young stars are correlated in position too. Gomez et al. (1993) studied the 2-point correlation function for stars in the local star-forming region Taurus. For 121 young stars, there was a power law distribution of the number of stars as a function of their separation, which means that the stars are hierarchically correlated. (A similar correlation might arise from an isothermal distribution of stars without any hierarchical structure, as in a relaxed star cluster, but the Taurus region is not like this.) The correlation in Taurus extended from $0.15''$ of arc separation to at least 2° separation – nearly 3 orders of magnitude. Larson (1995) extended this survey to smaller scales and found a break in the correlation at 0.04 pc. He suggested that smaller scales formed binary stars by fragmentation in clumps, and larger scales formed hierarchical groups by gas-related fragmentation processes, including turbulence.

Low mass x-ray stars in Gould's Belt (i.e., T Tauri stars) show a hierarchical structure in all-sky maps (Guillout et al., 1998). This means that large groupings of T Tauri stars contain smaller sub-groupings and these contain even smaller sub-sub groupings. This is a much bigger scale than the Taurus region studied by Gomez et al. (1993). There has been no formal correlation of the large-scale structure in x-ray stars yet. The all-sky coverage suggests that the Sun is inside a hierarchically clumped complex of young stars.

5 The Cartwright & Whitworth Q parameter

To study hierarchical structure in a different way, Cartwright & Whitworth (2004) introduced a parameter, Q. This is the ratio of the average separation in a minimum spanning tree to the average 2-point separation. For example, suppose there are 5 stars clustered together in one region with a typical separation of 1 unit, and another 5 stars clustered together in another region with a typical separation of 1 unit, and these two regions are separated by 10 units. Then the minimum spanning tree has 4 separations of 1 unit in each region and 1 separation of 10 units (for the two closest stars among those two regions), for an average of

$(8 \times 1 + 1 \times 10)/(8 + 1) = 2$ units length. The average separation for all possible pairs is counted as follows: there are 5 stars with separation from another star equal to about 1 in each region, so that means 5 stars taken 2 at a time in each region, or 10 pairs with a separation of 1 in each region, or 20 pairs with this separation total, plus each star in one group has a separation of 10 units from each star in the other group, which is 5×5 separations of 10 units. The average is $(20 \times 1 + 25 \times 10)/(20 + 25) = 6$. The ratio of these is $Q = 2/6 = 0.33$. Smaller Q means more subclumping because for multiple subgroups, the mean 2-point separation has a lot of distances equal to the overall size of the region, so the denominator of Q is large, but the minimum spanning tree has only a few distances comparable to the overall size of the system, one for each subgroup, and then the numerator in Q is small.

Bastian et al. (2009) looked at the correlated properties of stars in the LMC, using a compilation from Zaritsky et al. (2004). There were about 2000 sources in each of several age ranges on the color-magnitude diagram. Bastian et al. determined the zero-points and slopes of the two point correlation function for each different age. They found that younger regions have higher correlation slopes and greater correlation amplitudes, which means more hierarchical substructure. Most of this substructure is erased by 175 Myr. They also evaluated the Cartwright & Whitworth (2004) Q parameter and found a systematic decrease in Q with decreasing age, meaning more substructure for younger stars. Gieles et al. (2008) did the same kind of correlation and Q analysis for stars in the Small Magellanic Cloud, and found the same general result.

6 Hierarchies inside Clusters

In a hierarchically structured region, the average density increases as you go down the levels of the hierarchy to smaller and smaller scales. If there are dense star-forming cores at the bottom of the hierarchy, where the densities are largest and the sizes are smallest, then the fractional mass in the form of these cores increases as their level is approached. This is because more and more interclump gas is removed from the scale of interest as the densest substructures are approached. The fractional mass of cores is proportional to the instantaneous efficiency of star formation if the cores form stars. Therefore the local efficiency of star formation in a hierarchical cloud increases as the average density increases. The efficiency on the scale of a galaxy where the average density is low is $\sim 1\%$; on the scale of an OB association it is $\sim 5\%$, and in a cloud core where a bound cluster forms, it is $\sim 40\%$. Bound cluster formation requires a high efficiency so there is a significant gravitating mass of stars remaining after the gas leaves. It follows that in hierarchical clouds, the probability of forming a bound cluster is automatically highest where the density is highest. Star clusters are the inner bound regions of a hierarchy of stellar and gaseous structures (Elmegreen 2008).

Outside the inner region, stars that form are not as likely to be bound to each other after the gas leaves. Then there are loose stellar groups, unbound OB subgroups, OB associations, and so on up to star complexes. Flocculent spiral arms

and giant spiral-arm clouds are the largest scale on which gravitational instabilities drive the hierarchy of cloud and star-formation structures.

The hierarchy of young stellar structure continues inside bound clusters as well. Smith et al. (2005) found several levels of stellar subclustering inside the rho-Ophiuchus cloud, and Dahm & Simon (2005) found 4 subclusters with slightly different ages (± 1 Myr) in NGC 2264. Feigelson et al. (2009) observed X-rays from young stars in NGC 6334. The x-ray maps are nearly complete to stars more massive than 1 $M_\odot$ and their distribution is hierarchical, with clusters of clusters inside this region. Gutermuth et al. (2005) studied azimuthal profiles of clusters and found that they have intensity fluctuations that are much larger than what would be expected from the randomness of stellar positions; the stars are sub-clustered in a statistically significant way. Sánchez & Alfaro (2009) measured the fractal dimension and hierarchical-Q parameter for 16 Milky Way clusters, using the ratio of cluster age to size as a measure of youth. They found that stars in younger and larger clusters are more clumped than stars in older and smaller clusters. Greater clumping means they have lower Q and lower fractal dimension. Schmeja et al. (2008) measured Q for several young clusters. For IC 348, NGC 1333, and Ophiuchus, Q is lower (more clumpy) for class 0/1 objects (young) than for class 2/3 objects (old). Among four of the subclumps in Ophiuchus, Q is lower and the region is more gassy where class 0/1 dominates; Q is also lower for class 0/1 alone than it is for class 2/3 in Ophiuchus.

Pretellar cores are spatially correlated too. Johnstone et al. (2000) derived a power-law 2-point correlation function from $10^{3.8}$ AU to $10^{4.6}$ AU for 850μm sources in Ophiuchus, which means they are spatially correlated in a hierarchical fashion. Johnstone et al. (2001) found a similar power-law from $10^{3.6}$ AU to $10^{5.1}$ AU for 850μm sources in Orion. Enoch et al. (2006) showed that 1.1 μm pre-stellar clumps in Perseus have a power-law 2-point correlation function from $10^{4.2}$ AU to $10^{5.4}$ AU. Young et al. (2006) found similar correlated structure for pre-stellar cores from $10^{3.6}$ AU to 10^5 AU in Ophiuchus. These structures could go to larger scales, but the surveys end there.

In summary, clusters form in the cores of the hierarchy of interstellar structures and they are themselves the cores of the stellar hierarchy that follows this gas. Presumably, this hierarchy comes from self-gravity and turbulence. Gas structure continues to sub-stellar scales. The densest regions, which are where individual stars form, are always clustered into the next-densest regions. Stars form in the densest regions, some independently and some with competition for gas, and then they move around, possibly interact a little, and ultimately mix together inside the next-lower density region. That mixture is the cluster. More and more sub-clusters mix over time until the cloud disrupts. Simulations of such hierarchical merging have been done by many groups, such as Bonnell & Bate (2006) and Maschberger et al. (2010). Because of hierarchical structure, the efficiency is automatically high on small scales where the gas is dense.

7 Clustered versus Non-clustered Star Formation

Barba et al. (2009) examined the giant star-forming region NGC 604 in M33 with NICMOS, finding mostly unclustered stars. Maíz-Apellániz (2001) categorized star formation regions according to three types: compact clusters with weak halos, measuring 50×50 pc^2, compact clusters with strong halos measuring 100×100 pc^2, and hierarchical, but no clusters, called "Scaled OB Associations" (SOBAs), measuring 100×100 pc^2. Why do stars form in clusters some of the time but not always?

The occurrence of bound clusters in star forming regions could depend on many factors, but the pressure of the region relative to the average pressure should be important. Higher pressure regions should produce proportionally more clusters. Recall, that Elias, Alfaro & Cabrera-caño (2009) found a higher clustering fraction for the high-pressure Orion region compared to the low-pressure Sco-Cen region. One reason for a possible pressure dependence was discussed in Elmegreen (2008) and is reviewed here.

Turbulence produces a log-normal density probability distribution function (Vazquez-Semadeni, 1994; Price et al., 2010), and this corresponds to a log-normal cumulative mass fraction $f_{\rm M}(>\rho)$, which is the fraction of the gas mass with a density larger than the value ρ. This is a monotonically decreasing function of ρ. If the densest clumps have a density $\rho_{\rm c}$, and the star formation rate per unit volume is the dynamical rate for all densities with an efficiency (star-to-gas mass fraction) that depends on density, i.e., $SFR = \epsilon(\rho)\rho\,(G\rho)^{1/2}$, then the mass fraction of the densest clumps inside a region of average density ρ is

$$\epsilon(\rho) = \epsilon_{\rm c}\,(\rho_{\rm c}/\rho)^{1/2}\,[f_{\rm M}(>\rho_{\rm c})/f_{\rm M}(>\rho)]\,. \tag{7.1}$$

This function $\epsilon(\rho)$ increases with ρ for intermediate to high density. If stars form in the densest clumps with local efficiency $\epsilon_{\rm c}$ (~ 0.3), then $\epsilon(\rho)$ is the efficiency of star formation, i.e., the mass fraction going into stars for each average density. Bound clusters form where the efficiency is highest, and this is where the average density is highest. If we consider the density where $\epsilon(\rho)$ exceeds a certain minimum value for a bound cluster, then most star formation at this density or larger ends up in bound clusters.

Note that the observation of cluster boundedness appears to be independent of cluster mass and therefore independent of the presence of OB stars in the cluster. Bound clusters with highly disruptive OB stars form in dense cloud cores, just like clusters without these stars. The efficiency of star formation is therefore not related in any obvious way to the presence or lack of disruptive stars. The implication is that essentially all of the stars in a cluster form before OB-star disruption occurs. Perhaps the highly embedded nature of OB star formation, in ultracompact HII regions, for example, shields the rest of the cloud core from disruption for a long enough time to allow the lower mass cores to collapse into stars.

The pressure dependence for cluster boundedness arises in the theory of Elmegreen (2008) because at a fixed density for star formation, the slope of the $f_{\rm M}(>\rho)$

curve decreases for higher average density (the log-normal shifts to higher density), and the slope also decreases for higher Mach number because the log-normal gets broader. With a shallower slope at the density of star formation, the density where $\epsilon(\rho)$ exceeds the limit for bound cluster formation decreases, and the fraction of the mass exceeding this density increases. Thus forming a bound cluster happens at a lower density relative to the threshold for star formation when the pressure is high. A higher fraction of the gas then goes into bound clusters. The qualitative nature of this conclusion is independent of the details of the density pdf.

This discussion of cluster formation in a hierarchical medium assumes that the gas structure is already in place when star formation begins, and then the densest clumps, which are initially clustered together, form stars. The discussion can be made more dynamical if we consider that the denser regions fragment faster. This is what happens during a collapse simulation: the dense regions make more subcondensations and the low density regions collapse on to the dense regions. The result is a clustering of dense sub-condensations and a hierarchical clustering of stars.

8 Cluster Mass Functions

The cluster mass function is a power law and it is natural to look for explanations of this that are related to the other power laws in star formation, including the hierarchical structure. If we imagine a cloud divided hierarchically into clumps and sub-clumps, then the mass distribution function of the nodes in this hierarchy is $dN/d\log M \sim 1/M$, or $dn/dM \sim 1/M^2$, because there is an equal total mass in all levels ($MN[M]d\log M =$ constant). This is the same as the mass function for star clusters. Also in such a hierarchy, the probability that a mass between M and $2M$ is selected is proportional to $1/M$, as given by the number of levels and clouds at those levels having a mass in that range.

Cluster mass functions typically are a power law with a slope equal to this value, $dn/dM \sim M^{-\beta}$ for $\beta \sim 2$. This slope was found by Battinelli et al. (1994) for the solar neighborhood and Elmegreen & Efremov (1997) for the LMC, where the clusters were subdivided according to age. A second study of LMC clusters (Hunter et al., 2003) found the same slope for discrete cluster age intervals. It is important to consider clusters within a narrow age interval because older clusters are dimmer and the selection effects for clusters depend on their age. Zhang & Fall (1999) found $\beta = 1.95 \pm 0.03$ for young clusters in the Antenna galaxy, and $\beta = 2.00 \pm 0.08$ for old clusters. de Grijs & Anders (2006) looked at the LMC again and found $\beta = 1.85 \pm 0.05$ for various age intervals. de Grijs et al. (2003) found similar results in two other galaxies: $\beta = 2.04 \pm 0.23$ for NGC 3310 and $\beta = 1.96 \pm 0.15$ for NGC 6745.

The HII region luminosity function is about the same as the cluster mass function, having a slope of around -2 for linear intervals of luminosity. The first large study was by Kennicutt et al. (1989). Many other surveys have obtained about the same result (e.g., Banfi et al., 1993). Bradley et al. (2006) included 53 spiral galaxies and got a steeper slope at $\log L > 38.6$ (for L in erg s^{-1}), suggesting

that larger HII regions were density bounded, and they also got a steep fall-off at $\log L > 40$, suggesting an upper limit for cluster mass. The same general power law for HII regions has been obtained in detailed studies of individual galaxies (e.g., NGC 3389: Abdel-Hamid et al. (2003); M81: Lin et al. 2003; NGC 1569: Buckalew & Kobulnicky 2006; NGC 6384: Hakobyan et al. 2007; the Milky Way: Paladini et al. 2009).

There is growing evidence for an upper mass cutoff in the cluster mass function. In Gieles et al. (2006a,b), mass functions in M51 were fit to a double power law, i.e., with an increased slope at higher mass, or to a power law with $\beta = 2$ throughout and an upper mass cutoff of around $10^5\ M_\odot$. A power law with an exponential cutoff is a Schechter function, $dN/dM = M^{-\beta} \exp(-M/M_c)$ for cutoff mass M_c.

For several local galaxies, Larsen (2009) fit the brightest cluster and the 5th brightest cluster with a mass function having a cutoff. Larsen found that rich and poor spirals have about the same cluster mass functions, both with a cutoff, and that the cutoffs are independent of position in a galaxy. The origin of an upper mass limit for clustering is not known.

9 Summary

Gas is hierarchical in space and time, presumably because the gas is compressed by turbulent motions in a scale-free fashion. The self-gravitational force is scale free also at masses far above the thermal Jeans mass ($\sim 1\ M_\odot$). For a typical relationship between velocity dispersion and size that scales as $\sigma \propto R^{1/2}$, clouds of all masses at constant pressure have the same degree of gravitational self-binding.

Hierarchical cloud structure means that stars form in hierarchical patterns, and it follows then that the efficiency of star formation ($M_{\rm stars}/M_{\rm total}$) increases with the average density. Bound star clusters, which require a high efficiency, therefore form at high density. This explains at a very fundamental level why bound clusters form in the first place. Variations in the fraction of star formation that goes into bound clusters may be explained in the same way, with pressure playing an important role.

Hierarchical structure ensures that the clusters start with a mass function that is a power law with a slope close to -2. There could be an upper mass cut off.

References

Abdel-Hamid, H., Lee, S.-G., & Notni, P. 2003, JKAS, 36, 49

Banfi, M., Rampazzo, R., Chincarini, G., & Henry, R. B. C. 1993, A&A, 280, 373

Barba, R.H., et al. 2009, Ap&SS, 324, 309

Bastian, N., Gieles, M., Ercolano, B., & Gutermuth, R. 2009, MNRAS, 392, 868

Battinelli, P., Brandimarti, A., Capuzzo-Dolcetta, R. 1994, A&AS, 104, 379

Begum, A., Chengalur, J.N., & Bharadwaj, S. 2006, MNRAS, 372, L33

Bhatia, R. K., & Hatzidimitriou, D. 1988, MNRAS, 230, 215

Block, D. L., Puerari, I., Elmegreen, B. G., Elmegreen, D. M., Fazio, G. G., & Gehrz, R. D. 2009, ApJ, 694, 115

Block, D.L., Puerari, I., Elmegreen, B.G., & Bournaud, F. 2010, ApJ, 718, L1

Bonnell, I.A., & Bate, M.R. 2006, MNRAS, 370, 488

Bradley, T. R., Knapen, J. H., Beckman, J. E., & Folkes, S. L. 2006, A&A, 459, L13

Buckalew, B.A., & Kobulnicky, H.A. 2006, AJ, 132, 1061

Cartwright, A., & Whitworth A. P., 2004, MNRAS, 348, 589

Dahm, S.E., & Simon, T. 2005, AJ, 129, 829

de Grijs, R., Anders, P., Bastian, N., Lynds, R., Lamers, H. J. G. L. M., & O'Neil, E. J. 2003, MNRAS, 343, 1285

de Grijs, R. & Anders, P. 2006, MNRAS, 366, 295

de la Fuente Marcos, R., & de la Fuente Marcos, C. 2008, ApJ, 672, 342

de la Fuente Marcos, R. & de la Fuente Marcos, C. 2009a, ApJ, 700, 436

de la Fuente Marcos, R. & de la Fuente Marcos, C. 2009b, A&A, 500, L13

Dieball, A., Mller, H., & Grebel, E. K. 2002, A&A, 391, 547

Dutta, P., Begum, A., Bharadwaj, S., & Chengalur, J.N. 2008, MNRAS, 384, L34

Dutta, P., Begum, A., Bharadwaj, S., & Chengalur, J.N. 2009a, MNRAS, 397, L60

Dutta, P., Begum, A., Bharadwaj, S., & Chengalur, J.N. 2009b, MNRAS, 398, 887

Efremov, Y.N. 1995, AJ, 110, 2757

Efremov, Y. N., & Elmegreen, B. G. 1998, MNRAS, 299, 588

Eggen, O. J. 1989, Fund. Cosmic Physics, 13, 1

Elias, F., Alfaro, E. J., & Cabrera-Caño, J. 2009, MNRAS, 397, 2

Elmegreen, B.G. 2008, ApJ, 672, 1006

Elmegreen, B.G. 2010, in Star Clusters: Basic Galactic Building Blocks Throughout Time And Space, eds. R. de Grijs and J. Lepine, Cambridge: Cambridge Univ. Press, p. 3

Elmegreen, B. G., & Elmegreen, D. M. 1983, MNRAS, 203, 31

Elmegreen, B.G. & Efremov, Yu.N. 1996, ApJ, 466, 802

Elmegreen, B.G. & Efremov, Yu.N. 1997, ApJ, 480, 235

Elmegreen, B.G., Kim, S., & Staveley-Smith, L. 2001, ApJ, 548, 749

Elmegreen, D.M., Elmegreen, B.G., & Eberwein, K.S. 2002, ApJ, 564, 234

Elmegreen, B.G., Elmegreen, D. M., & Leitner, S. N. 2003, ApJ, 590, 271

Elmegreen, B.G., Elmegreen, D.M., Chandar, R., Whitmore, B., Regan, M. 2006, ApJ, 644, 879

Elmegreen, B.G, Galliano, E., & Alloin, D. 2009, ApJ, 703, 1297

Engargiola, G., Plambeck, R. L., Rosolowsky, E., & Blitz, L. 2003, ApJS, 149, 343

Enoch, M.L. et al. 2006, ApJ, 638, 293

Feigelson, E.D., Martin, A.L., McNeill, C.J., Broos, P.S., & Garmire, G.P. 2009, AJ, 138, 227

Feitzinger, J. V., & Galinski, T. 1987, A&A, 179, 249

Gieles, M., Larsen, S.S., Bastian, N., & Stein, I.T. 2006a, A&A, 450, 129

Gieles, M., Larsen, S.S., & Sheepmaker, R.A. 2006b, A&A, 446, L9

Gieles M., Bastian N., & Ercolano E. 2008, MNRAS, 391, L93

Gomez, M., Hartmann, L., Kenyon, S. J. & Hewett, R. 1993, AJ, 105, 1927

Guillout, P., Sterzik, M. F., Schmitt, J. H. M. M., Motch, C., Egret, D., Voges, W., & Neuhaeuser, R. 1998, A&A, 334, 540

Gutermuth, R.A., Megeath, S.T., Pipher, J.L., Williams, J.P., Allen, L.E., Myers, P.C., Raines, S.N. 2005, ApJ, 632, 397

Hakobyan, A. A., Petrosian, A. R., Yeghazaryan, A. A., & Boulesteix, J. 2007, Ap, 50, 426

Hatzidimitriou, D., & Bhatia, R. K. 1990, A&A, 230, 11

Hunter, D.A., Elmegreen, B.G., Dupuy, T.J., & Mortonson, M. 2003, AJ, 126, 1836

Ivanov, G.R. 2005, Pub. Astr. Soc. Rudjer Boskovic, 5, 75

Johnstone, D., Wilson, C.D., Moriarty-Schieven, G., Joncas, G., Smith, G., Gregersen, E., & Fich, M. 2000, 545, 327

Johnstone, D., Fich, M., Mitchell, G.F., & Moriarty-Schieven, G. 2001, ApJ, 559, 307

Kennicutt, R.C., Jr., Edgar, B. K., & Hodge, P.W. 1989, ApJ, 337, 761

Kharchenko, N. V., Piskunov, A. E., Röser, S., Schilbach, E., & Scholz, R.-D. 2005, A&A, 438, 1163

Larsen, S.S. 2009, A&A, 494, 539

Larson, R.B. 1973, MNRAS, 161, 133

Larson, R.B. 1981, MNRAS, 194, 809

Larson, R.B. 1982, MNRAS, 200, 159

Larson, R.B. 1991, in Fragmentation of Molecular Clouds and Star Formation, IAU Symposium 147, eds E. Falgarone, F. Boulanger, & G. Duvert, Dordrecht: Kluwer, 261

Larson, R.B. 1992, MNRAS, 256, 641

Larson, R.B. 1995, MNRAS, 272, 213

Lin, W., et al. 2003, AJ, 126, 1286

Maíz-Apellániz, J. 2001, ApJ, 563, 151

Maschberger, Th., Clarke, C. J., Bonnell, I. A., & Kroupa, P. 2010, MNRAS, 404, 1061

Montenegro, L., Yuan, C., & Elmegreen, B. G. 1999, ApJ, 520, 592

Paladini, R., De Zotti, G., Noriega-Crespo, A., & Carey, S. J. 2009, ApJ, 702, 1036

Piskunov, A. E., Kharchenko, N. V., Röser, S., Schilbach, E., & Scholz, R.-D. 2006, A&A, 445, 545

Price, D.J., Federrath, C., & Brunt, C.M. 2010, ApJL, in press arXiv:1010.3754

Sánchez, N., & Alfaro, E.J. 2008, ApJS, 178,1

Sánchez, N., & Alfaro, E.J. 2009, ApJ, 696, 2086

Scalo, J.S. 1985, in Protostars and Planets II, ed. D.C Black and M. S. Matthews, (Tucson: Univ. of Arizona Press), p. 201

Scalo, J. 1990, in Physical Processes in Fragmentation and Star Formation, eds. R. Capuzzo-Dolcetta, C. Chiosi, & A. Di Fazio, Dordrecht: Kluwer, p. 151

Scheepmaker, R. A., Lamers, H. J. G. L. M., Anders, P., & Larsen, S. S. 2009, A&A, 494, 81

Schmeja, S., Kumar, M. S. N., & Ferreira, B. 2008, MNRAS, 389, 1209

Smith, M.D., Gredel, R., Khanzadyan, T. et al. 2005, MmSAI, 76, 247

Stanimirovic, S., Staveley-Smith, L., Dickey, J.M., Sault, R.J. & Snowden, S.L. 1999, MNRAS, 302, 417

Stanimirovic, S., Staveley-Smith, L., van der Hulst, J. M., Bontekoe, T.J. R., Kester, D. J. M., & Jones, P. A. 2000, MNRAS, 315, 791

Vazquez-Semadeni, E. 1994, ApJ, 423, 681

Willett, K. W., Elmegreen, B. G., & Hunter, D. A. 2005, AJ, 129, 2186

Young, K.E. et al. 2006, ApJ, 644, 326

Zaritsky, D., Gonzalez, A,H., & Zabludoff, A.I. 2004, ApJ, 613, L93

Zhang, Q., & Fall, S.M. 1999, ApJ, 527, L81

Zhang, Q., Fall, S. M., & Whitmore, B. C. 2001, ApJ, 561, 727

Ecole Evry Schatzman 2010: Star Formation in the Local Universe
Eds. C. Charbonnel & T. Montmerle
EAS Publications Series, 2011

TRIGGERED STAR FORMATION

Bruce G. Elmegreen[1]

Abstract. Triggered star formation in bright rims and shells is reviewed. Shells are commonly observed in the Milky Way and other galaxies, but most diffuse shells seen in HI or the infrared do not have obvious triggered star formation. Dense molecular shells and pillars around HII regions often do have such triggering, although sometimes it is difficult to see what is triggered and what stars formed in the gas before the pressure disturbances. Pillar regions without clear age gradients could have their stars scattered by the gravity of the heads. Criteria and timescales for triggering are reviewed. The insensitivity of the average star formation rate in a galaxy to anything but the molecular mass suggests that triggering is one of many processes that lead to gravitational collapse and star formation.

1 Introduction: Large-Scale Shells

High resolution images of nearby spiral galaxies show large dust and gas bubbles in the spiral arms (Fig. 1; see also Fig. 3 in Lecture 2). Their radii are often larger than the gas scale heights, so these are unlikely to be spheres; they are more like rings in the disk. There are also feathers, comets, and other fine-scale dust structures in optical images – all indicating recent dynamical processes. Sometimes there are small bubbles inside large bubbles, and there are generally more bubbles near the spiral arms than in the interarm regions. The interarm also contains dust streamers, and many of these look like old bubbles left over from more active times in the arms.

Gould's Belt contains the Local Bubble, studied recently by Lallement et al. (2003) using Na I absorption clouds near the Sun. This local bubble is also a source of diffuse x-ray emission from hot gas (Snowden et al., 1998). Presumably the energy came from hot stars in the Sco-Cen association (Breitschwerdt & de Avellez, 2006).

[1] IBM T. J. Watson Research Center, 1101 Kitchawan Road, Yorktown Heights, New York 10598 USA, bge@us.ibm.com

DOI: (will be inserted later)

Large bubbles in the Milky Way are also evident from IR maps of the sky. Könyves et al. (2007) used IRAS 60μm and 100μm images to identify Milky Way bubbles. They reported that the bubble volume filling factor in the inner galaxy is around 30%, and in the outer galaxy it is around 5%. Ehlerová & Palouš (2005) catalogued HI shells in the Milky Way using the Leiden-Dwingeloo Survey. They found a volume filling factor of 5%, a mean age of 8.4 Myr, and a ratio of age to filling factor equal to 170 Myr. This latter timescale is the time for the whole interstellar volume (not mass) to be cycled through one or another HI shell. This is 10 times faster than the time for molecular gas to be converted into stars. Since the shells observed by Ehlerová & Palouš are atomic, this ISM processing would seem to be independent of the molecular cloud population. The GMCs have a low volume filling factor and the HI shells occupy the space between them. A significant fraction of the HI shell mass can come from GMC disruption in the inner galaxy where the molecular fraction is high.

The LMC is also filled with large shells (Goudis & Meaburn, 1978). The largest, LMC4, has no obvious cluster or OB association in the center, although

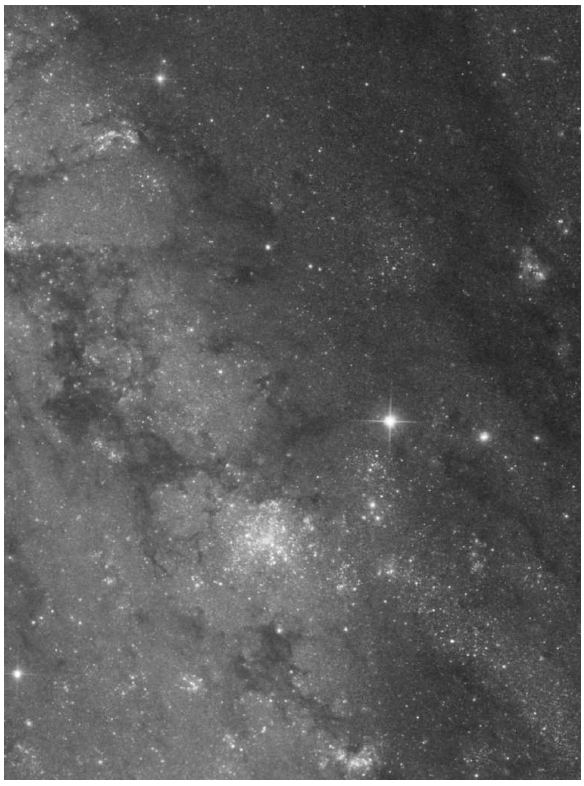

Fig. 1. Region of the galaxy M51 viewed with the ACS camera of HST, showing bubbles.

there are A-type stars suggesting a $\sim$ 30 Myr old age (Efremov & Elmegreen, 1998). It has pillars at the edge with young star formation, and an arc of young stars without gas in the center, called Constellation III (McKibben Nail & Shapley, 1953). Yamaguchi et al. (2001) studied the star formation in this region, pointing out GMCs and young clusters all along the edge of the shell and suggesting these were triggered.

IC 10 is another small galaxy filled with HI holes and shells. Wilcots & Miller (1998) found Hα at the edges of the shells and discussed these young regions as triggered star formation. Similarly, the small galaxy IC 2574 has a giant shell with an old central cluster and triggered young stars on edge (Walter & Brinks, 1999; Connon et al., 2005).

2 Shell Expansion

Expanding shells are most commonly made by stellar pressures in the form of HII regions, supernovae, and winds. If we write the expansion speed as $dR/dt \sim (P/\rho)^{1/2}$ for an isothermal shock, then the radius varies as a power law in time if the pressure P is a function of radius R and the density ρ is uniform. For an HII region, $P = 2.1nkT$ where $n = (3S/4\pi R^3\alpha)^{1/2}$ for ionizing luminosity S in photons per second and recombination rate α to all but the ground state. Then $P \propto R^{-3/2}$. For supernovae, $P \sim 3E/4\pi R^3$ for the energy conserving, non-radiative, phase. For a wind, $P \sim 3E(t)/4\pi R^3$, where the energy increases with time as $E = Lt$.

These three pressure-radius relations give three different radius-time expansion laws, $dR/dt \propto R^{-3/4}$ gives $R \propto t^{4/7}$ for a Strömgren sphere, $dR/dt \propto R^{-3/2}$ gives $R \sim t^{2/5}$ for the Sedov phase of a supernova, and $dR/dt \propto t^{1/2}R^{-3/2}$ gives $R \propto t^{3/5}$ for a steady wind or continuous energy supply from multiple supernovae in an OB association (Castor et al., 1975).

There are many complications to these solutions. External pressure is always present, slowing down the bubbles. External pressure $P_{\rm ext}$ enters the expression as $dR/dt = ([P - P_{\rm ext}]/\rho)^{1/2}$ with $P_{\rm ext}$ $\sim$constant. The solution is not a power law in this case. A second complication is the momentum in the moving shell. When this is important, the equation of expansion is really $d(4\pi R^3 v\rho/3)/dt = 4\pi R^2(P - P_{\rm ext})$. Shell momentum makes the shell move faster at a given radius than in the case without momentum. There are also diverse shock jump conditions depending on the importance of magnetic fields and the equation of state for the shocked gas, such as adiabatic or isothermal, or whether the full energy equation is used to determine the post-shock temperature.

We can see how important external pressure is to these solutions by finding the fraction of shells that are at a pressure significantly above the external value. As noted above, each source has solutions $R(t)$ and $P(R)$, which can be re-written into a solution for pressure versus time, $P(t)$. Thus there is a relation for the volume as a function of pressure, $V(P)$. For a constant rate n_0 of making bubbles, $n(P)dP = n_0 dt$. Therefore $n(P) \propto dt/dP$. The volume filling factor is $f(P) = n(P)V(P)$. Now we see that for HII regions, $f(P) \propto P^{-4.17}$; for winds, $f(P) \propto P^{-4.5}$, and for supernovae, $f(P) \propto P^{-5.2}$. For all of these, approximately, $f(P)dP \propto AP^{-4.5}dP$

for some constant A. If all of the volume is filled, then $1 = \int f(P)dP$, and the average pressure is related to the minimum pressure as $P_{\rm ave} = 1.4P_{\rm min}$, which means $f(P) = 1.15(P/P_{\rm ave})^{-4.5}/P_{\rm ave}$. Thus, the probability that any of these regions has a pressure exceeding 10 times the average, $f(P > 10P_{\rm ave})$, is $0.31 \times 0.1^{3.5} \sim 10^{-4}$; similarly, $f(P > 2P_{\rm ave}) \sim 0.03$. Evidently, most pressure bursts from HII regions, winds and supernovae are within twice the average ISM pressure for most of their lives. Therefore the external pressure is important for them. Kim, Balsara & Mac Low (2001) ran numerical simulations of the ISM and found that most of the time, the pressure stayed within a factor of 2 of the average value.

The probability distribution function for pressure also suggests that the largest pressure bursts are close-range and short-lived. Thus significant over-pressures from stellar sources are most likely to occur close to those stars, as in an adjacent cloud. Most of the giant IR and HI shells discussed above are drifting by momentum conservation.

3 Triggering: Bright Rimmed Clouds and Pillars

HII regions interact with their neighboring molecular clouds by pushing away the lower density material faster than the higher density cloud cores. This leads to bright rims and pillars. Most HII regions contain these shapes, as they are commonly observed in Hubble Space Telescope images of nebulae. Triggered star formation in the dense heads of pillars has been predicted (e.g., Klein, Sandford & Whitaker, 1980) and observed for many years (e.g., Sugitani et al., 1989). Here we review some recent observations.

Recent simulations of bright rim and pillar formation are in Mellema et al. (2006), Miao et al. (2006), and Gritschneder et al. (2009). In a large HII region,

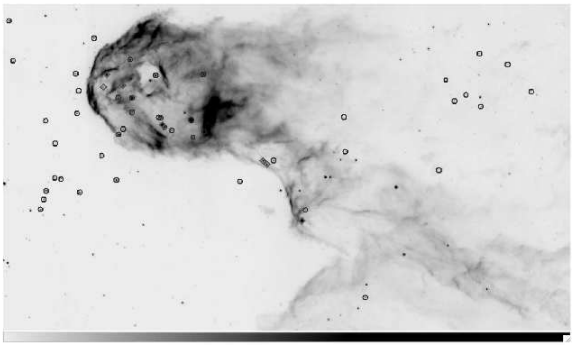

Fig. 2. A pillar in IC 1396 viewed at 8μm with the Spitzer Space Telescope. Class I sources (the youngest) are identified by diamond shapes. There are three at the front of the head, one near the back part of the head, two on the lower part of the pillar and another in a shelf nearby (from Reach et al. (2009).

there can be many bright rims with star formation in them. A good example is 30 Dor in the LMC, which has bright-rims that look like they have triggered star formation in many places (Walborn, Maíz-Apellániz & Barbá, 2002).

IC 1396 is an HII region with a shell-like shape. The radius is 12 pc, and the expansion speed is 5 km s^{-1}, making the expansion time 2.5 Myr (Patel et al., 1995). The shell contains several bright rims and pillars around the edge that all point to the sources of radiation. In optical light, few embedded stars can be seen, but in the infrared there are often embedded stars.

The stellar content of the large pillar in IC 1396 has been studied by Reach et al. (2009; see Figure 2). Several Class I protostars are located in the main head and in a shelf off the main pillar. Class II stars are scattered all over the region with no particular association to the cloud. The Class I stars recently formed in the pillar, and considering that they are much younger than the HII region, they could have been triggered.

Getman et al. (2007) observed IC 1396N, another bright rim in the same region, in x-ray and found an age sequence that suggests triggering from south to north, into the rim. There are class III and class II stars around the rim and class I/0 stars inside. Beltrán et al. (2009) did a JHK survey of the same bright rim and found few NIR-excess sources and no signs of clustering toward the southern part of the rim. They also found no color or age gradient in the north-south direction. They concluded there was no triggering but perhaps there was a gradient in the erosion of gas around protostars. Choudhury et al. (2010) observed the region with Spitzer IRAC and MIPs and suggested there was an age sequence with the younger stars in the center of the bright rim and the older stars near the edge. They derived a propagation speed into the rim of $0.1 - 0.3$ km s^{-1}.

The pillars of the Eagle Nebula, M16, are among the most famous cloud structures suggestive of triggering. Several young stars appear at the tips. It is difficult to tell if these stars were triggered by the pressures that made the pillars, or if they existed in the head regions before the HII pressure swept back the periphery. Triggering requires that the pillar stars are much younger than the other stars in the region. Some exposure of existing stars could be possible if there is a wide range of ages among the pillar and surrounding stars.

Sugitani et al. (2002) found Type I sources near the pillar heads in M16 and older sources all around the pillars. They suggested there was an age sequence within the pillar. Fukuda et al. (2002) observed M16 in ^{13}CO, $C^{18}O$, and 2.7 mm emission, finding a high density molecular core at the end of the pillar, as expected from HII region compression. However, Indebetouw et al. (2007) suggested that the young objects in the area are randomly distributed and not triggered. They showed the distribution of protostars in various stages of accretion and saw no clear patterns with age. Thus the issue of triggering in the M16 pillars seems unresolved.

Guarcello et al. (2010) found a different age sequence in M16: the stars in the northwest part of the whole HII region are younger than the stars in the southeast part. They suggested that a 200 pc shell triggered both M16 and M17 3 Myr ago on much larger scales.

IC 5146 is a filamentary cloud with low-level star formation at one end (Lada, Alves & Lada, 1999). It is not in an HII region and the source of the structure and pressure to shape it is not evident. It looks like it was formerly a diffuse cloud that was compressed at one end by a supernova. The ends of a filamentary cloud are the most susceptible parts to this kind of random disturbance.

Hosokawa & Inutsuka (2007) studied molecule formation in compressed shells around HII regions and suggested that H_2 could form without bright CO emission during the expansion of the shell into a cold neutral medium. They found an example of this in the shell around the W3-4-5 region. There is cold HI and perhaps unobserved H_2, without any evident CO. They proposed that this is an intermediate stage in the collapse of a swept up shell and the site for future triggered star formation.

The Ophiuchus cloud core was swept back by pressures from the Sco-Cen association (de Geus, 1992). Star formation in the rho Oph region could have been triggered at the same time. A large-scale dust map of the whole region is in Lombardi et al. (2008; see Figure 3). There are many protostars and dense cores (e.g., Kirk, Ward-Thompson & André, 2005) in what looks like a giant pillar. Sco-Cen is off the field to the upper right.

The Carina nebula has many bright rimmed clouds and pillars that were recently studied by Smith (2010). They note that the young stars lag the bright rims, as if they were left behind in an advancing ionization front of cloud destruction.

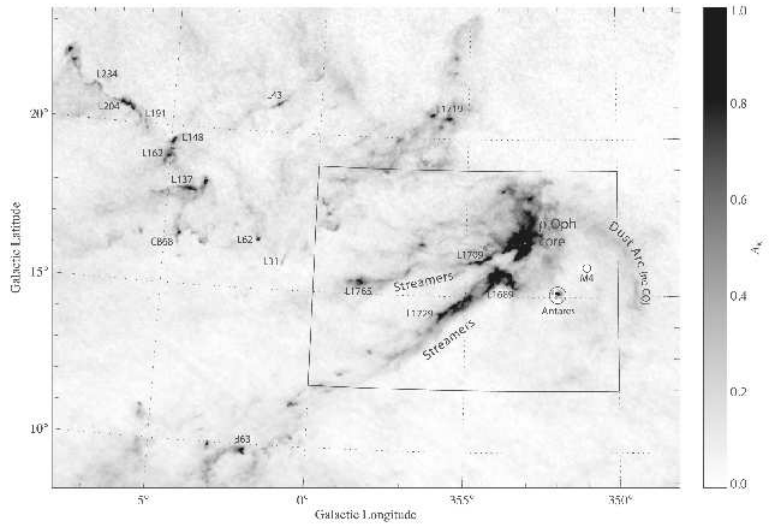

Fig. 3. Large-scale dust map of the Ophiuchus region, from Lombardi, Lada & Alves (2008).

4 Age Sequences in Bright Rims

Several of the references above look for or find age sequences of stars along the axis of a bright rim. Sugitani, Tamura & Ogura (1995) pioneered this. At first, such a sequence seems obvious because the HII region is expanding, so position correlates with time. However, the bright-rim heads are usually more massive than the stars and the stars should be gravitationally attracted to the heads. If the head acceleration by gas pressure is less than their internal acceleration by gravity, then the embedded stars will get pulled along with the heads as the heads move. There would be little exposure of the stars in that case. To accelerate the head faster than the internal gravitational acceleration means that the pressure difference between the front and the back side has to exceed the internal gravitational acceleration multiplied by the head column density. Both of these quantities are essentially the internal self-gravitational binding energy of the head if the head is virialized, and therefore also the internal turbulent energy density. In that case, the head has to be accelerated faster than the square of its turbulent velocity dispersion divided by its radius. Such a larger acceleration could occur when the initially low-density gas is first compressed into a comet head by the HII region. Once the entire head is compressed and star formation occurs in the dense gas, the inside of the head will be close to pressure equilibrium with the outside ionization front, and the relative acceleration will decrease.

A description of such pressure equilibrium and the resulting acceleration is given by Bertoldi & McKee (1990). In their equation 5.10, they write the ratio of the self-gravitational acceleration inside the head to the acceleration of the whole head by the rocket effect as

$$\frac{g_{\rm grav}}{g_{\rm rocket}} \sim 2\left(\frac{M_{\rm cl}}{M_{\rm Jeans}}\right)^{2/3} \tag{4.1}$$

for a non-magnetic head, and

$$\frac{g_{\rm grav}}{g_{\rm rocket}} \sim \left(\frac{M_{\rm cl}}{M_{\Phi}}\right)^{2} \tag{4.2}$$

for a magnetic head. Here, $M_{\rm cl}$ is the cloud head mass, $M_{\rm Jeans} = 1.18\sigma_{\rm cl}^4/(G^3P_{\rm cl})^{1/2}$ and $M_\Phi = 0.12\Phi/G^{3/2}$ are the critical (or maximum) cloud masses for stability without and with a magnetic field, respectively; Φ is the total magnetic flux in the cloud. The pressure at the ionized surface of the cloud enters the expression for $M_{\rm Jeans}$ and is

$$\frac{P_{\rm cl}}{k} = 2.45\times10^7[S_{49}/(R_{\rm cl,pc}R_{\rm pc}^2)]^{1/2}\ {\rm cm}^{-3}K \text{ if } (\psi > 10) \tag{4.3}$$

$$= 1.65\times10^9(S_{49}/R_{\rm pc}^2)\ {\rm cm}^{-3}K \text{ if } (0.3 < \psi < 10) \tag{4.4}$$

for dimensionless parameter ψ,

$$\psi = \alpha F_{\rm II}R_{\rm cl}/\sigma_{\rm II}^2 = 5.15\times10^4\frac{S_{49}R_{\rm cl,pc}}{R_{\rm pc}^2}. \tag{4.5}$$

In these expressions, the recombination rate to all but the ground state is α, the incident ionizing flux is $F_{\rm II}$ in photons cm^{-2} s^{-1}, the ionizing luminosity is S_{49} in photons s^{-1}, the cloud radius is $R_{\rm cl,pc}$ in pc, the distance to the ionizing source is $R_{\rm pc}$, in pc, the velocity dispersion in the cloud is $\sigma_{\rm cl}$, and the velocity dispersion in the HII region is $\sigma_{\rm II}$.

These equations suggest that if the cloud head requires gross instability for a star to form, i.e., $M_{\rm cl} > M_{\rm Jeans}$ or $M_{\rm cl} > M_\Phi$ (or, $M_{\rm cl} > M_{\rm Jeans} + M_\Phi$ in McKee (1989), then the internal gravitational acceleration in the head is always greater than the rocket acceleration. Thus the stars that form in the head should follow the head along as it accelerates away from the HII region. Why are the stars "left behind" in this case?

Another consideration is that the side of the dense core facing the HII region could be continuously peeled away by the ionization. The speed of this peeling is determined by the incident flux. After pressure equilibrium, a D-type ionization front enters the compressed neutral gas; "D" stands for density-bounded, i.e., the ionizing radiation is stopped by gas absorption (Spitzer, 1978). The speed of such a front into the dense gas is $\sigma_{\rm cl}^2/[2\sigma_{\rm II}]$. Because $\sigma_{\rm II} >> \sigma_{\rm cl}$, this D-front speed is always much less than $\sigma_{\rm cl}$. The orbit speed of a newly formed star inside the head is of order $\sigma_{\rm cl}$, however, for a self-gravitating head. Thus the speed at which the ionized side of the pillar gets peeled away is always much less then the embedded stellar speed. Thus, stars should not be exposed by ionization either.

Evidently, for both the rocket effect and ablation by ionization, stars forming in an unstable head should should continuously fall back into the head center faster than the surface of the head moves away from the source of ionization. This makes the exposure of young stars and their age gradients difficult to understand. It could explain, however, why age gradients are seldom obvious – the triggered stars scatter around the head by gravitational forces.

One solution to this problem is that the head is stable on a large scale with $\sigma_{\rm cl}$ equal to some turbulent speed that is larger than the sound speed, or perhaps with magnetic support, and yet inside of the head, there are local dense clumps that are unstable in the sense that their masses are larger than the thermal Jeans mass after the magnetic field has diffused out. In these cases, it might be possible that $M_{\rm core} > M_{\rm Jeans,thermal}$ for localized star formation while at the same time $g_{\rm grav} < g_{\rm rocket}$ for exposure of the star after it forms.

Another model of triggered star formation is that there is a pre-existing pillar-like shape with multiple clumps aligned to the HII region. Then the compression front moves along the pillar from clump to clump, triggering gravitational instabilities as it goes. The exposure of the stars would follow the erosion of each clump, compressed one after another.

Of course it is possible that the stars near the head were not triggered. A key observation for triggering will be the velocities of the young stars near the head in comparison to the head velocity. If the stars are moving much slower than the head, then they could have formed before the compression and rocket-like acceleration.

Simulations by Dale et al. (2007b) of triggered star formation in numerous

dense clumps of a pre-existing molecular cloud indicate the difficulty in distinguishing between stars that formed previously and were exposed by clump ionization or motion, and stars that were triggered by the ionization pressure. In this study, the additional amount of star formation that was from the triggering alone was only $\sim 30\%$.

5 Shell Expansion: Collect and Collapse

Zavagno et al. (2006) studied star formation in the Milky Way source W 79 (Fig. 4). It has a 1.7 Myr old shell with gravitationally collapsed regions 0.1 Myr old along the perimeter. This is an example of star formation triggering by the gravitational collapse of swept-up gas around an older cluster or OB association. Sh2-219 is a similar region (Deharveng et al., 2006). There is O9.5V star in a centralized HII region, and a CO cloud, K-band embedded cluster, Ultra-compact HII region, and Herbig Be star at the edge.

Deharveng et al. (2010) recently studied 102 bubbles and triggered star formation using the Spitzer-GLIMPSE and MIPSGAL surveys for the IR, the MAGPIS and VGPS surveys for the radio continuum, and the ATLASGAL survey at 870 μm for cold dust emission. They found that 86% of the bubbles contain HII regions, and among those with adequate resolution, 40% have cold dust along their bor-

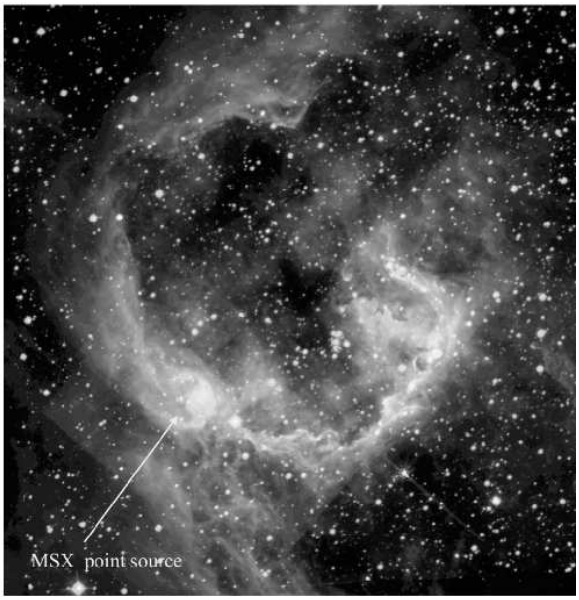

Fig. 4. Milky Way region W 79, consisting of a shell with dense clouds and star formation at the edge, from Zavagno et al. (2006).

ders, presumably accumulated during the bubbles' expansions. Eighteen bubbles have either ultracompact HII regions or methanol masers in the peripheral dust, indicating triggering. They categorized their results into several types of triggering. Star formation that occurs in pre-existing cloud condensations is distinctive because the clouds protrude into the bubble cavity like bright rims; 28% of the resolvable shells are like this. Star formation that occurs by the collapse of swept-up gas does not protrude but is fully in the shell. That is because it is comoving with the shell. In fact, clumps forming by gravitational collapse in a shell could eventually protrude out of the front of the shell because their higher column densities makes them decelerate slower than the rest of the shell (Elmegreen, 1989). If this is observed, then the relative position of a triggered clump and the shell around it should indicate their relative speeds and the time when the clump first formed.

Beerer (2010) studied Cygnus X North with Spitzer IRAC, classifying stars according to their IR spectral ages. They found that younger objects are in filaments that look compressed. Triggering of those stars was suggested.

Desai (2010) examined all 45 known supernova remnants in the LMC and looked for associations with young stellar objects and with GMCs that have no YSOs. Seven SNR were associated with GMCs and YSOs, 3 SNRs were with YSOs and no GMCs, and 8 SNRs were with GMCs and no YSOs. For the 10 SNRs with YSOs, only 2 have YSOs that are clearly associated with the SN shell, but in these cases, the SNe are younger than YSOs, so the YSOs could not have been triggered. Desai et al. concluded that SNe are too short-lived for triggering.

6 General Aspects of Triggering

Gas expands away from long-lived pressure sources like HII regions and OB association bubbles. If the expansion scale is smaller than the scale of a single cloud or the distance to a nearby cloud, then pillars and bright rims form by the push-back of interclump gas. In this case, star formation is a relatively fast process that works by squeezing the pre-existing dense gas. The velocity of the triggered stars is smaller than the overall shell expansion speed. The time delay between the beginning of the pressure source and the formation of new stars is the time for the pressure disturbance to reach the pre-existing cloud, i.e., the HII region expansion time, plus the time for the pressure to implode the cloud, which is relatively fast.

If the expansion scale is larger than the scale of a single cloud, then shells form by the push-back of most nearby gas. A cavity then forms with accumulated dense gas at the edge. This process of triggering is relatively slow because new clumps have to form by gravitational instabilities in the swept-up gas. The timescale for collapse and the properties of shells when they collapse were investigated by Elmegreen et al. (2002) using collapse criteria in Elmegreen (1994). They ran several thousand models of expanding shells in rotating, shearing galaxies and found various trends with environmental factors. The basic time scale for triggering was

$$t \sim 4\xi^{1/10}(2\pi G\rho_0)^{-1/2}, \tag{6.1}$$

where $\xi = \sigma^5/GL$ for source luminosity L and sound speed σ in the shell, and for pre-shell density ρ_0. They also found that the probability of collapse, or the fraction of shells that collapse, f, depends on the Toomre Q parameter for all possible variations in environment (see Lecture 1). The relation is $f \sim 0.5 - 0.4 \log_{10} Q$.

Simulations of shell formation and collapse around HII regions were made by Hosokawa & Inutsuka (2005, 2006a,b) and Dale et al. (2007a). Hosokawa & Inutsuka (2006a) found that shells driven into molecular clouds at typical densities have time to fragment and form new stars. They showed that at low ambient densities, the fragmentation can occur before CO forms, but at high densities, the shell is primarily CO. Hosokawa & Inutsuka (2006b) considered the minimum stellar mass that drives an expansion in which triggered star formation produces a second generation mass comparable to or larger than the first star; this stellar mass is around 20 $M_\odot$ for a pre-shock density of 100 cm^{-3}. Dale et al. (2007a) ran several simulations of an expanding HII region into a molecular cloud and compared the resulting radii and times for collapse with the analytical theory by Whitworth et al. (1994), which represented the numerical results well.

For the collect and collapse process, the velocity of triggered stars in the swept-up region can be large, $\sim (P/\rho_0)^{1/2}$ for driving pressure P and ambient density ρ_0. Evidence for triggering involves the causality condition: the triggering distance, age difference, and relative velocity of the triggered stars compared to the pressure-driving stars has to satisfy the relationship that the distance equals the velocity times the time. The triggered stars have to be much younger than the pressure-driving stars, and there has to be a clear age bifurcation into triggering star ages and triggered star ages, in order to be certain that triggering has occurred. Without a clear age difference, the suspected triggered stars could be part of the overall star formation process in the first generation, even if they are located in a compressed clump near the edge of the pressurized region.

Simulations of star formation triggered by ionization pressure have been discussed by Dale et al. (2005, 2007b) and Gritschneder et al. (2009). These simulations run for too short a time to generate an expanding coherent shell and form stars by the collect and collapse mechanism. Triggering instead is by the forced compression of pre-existing clumps. Because stars are forming in these clumps anyway, the excess star formation from triggering is small. Longer-time simulations could show more triggering in the collect and collapse scenario. As mentioned above, the timescale has to be several times the dynamical time in the pre-shock material. This is a problem for clouds that are not magnetically supported because they will collapse anyway in that time, even without compression. Thus triggering, as observed in shells, requires stability before the compression arrives, presumably from magnetic forces, and instability after the compression, presumably from enhanced magnetic diffusion in the compressed region combined with a greater surface pressure for the given cloud mass.

Thick shells should differ from thin shells in their stability properties because the gravitational forces in the shell are diluted by thickness when it is large, as discussed for galactic disks in Section 1.1 of Lecture 1. Wünsch (2010) studied the

thick shell case for shells that do not accumulate material as they expand, but are bound on both sides by thermal pressure.

7 ISM Energy Sources that may Trigger Star Formation

There are many energy sources for the ISM but only a few are likely to trigger star formation. The essential condition is that the energy source has to change a cloud from stable to unstable. Usually this requires some kind of compression, the compressed mass has to exceed an unstable mass, and the compressive force has to last for a time comparable to the collapse time in the compressed region. As mentioned above, individual supernova seem too short-lived to trigger star formation in the ambient ISM, even though they play an important role in energizing the ISM. More important are the HII regions, stellar winds bubbles, and multiple supernovae that occur in OB associations and star complexes. Another long-range and long-lived source of compression is a spiral density wave.

8 Summary

As we have seen over the last four lectures, star formation can be initiated by a variety of processes, including spontaneous gravitational instabilities in the combined stellar and gaseous medium, occasional cloud collisions, especially in density-wave shocks, and triggered gravitational instabilities in compressed regions ranging from spiral-arm dust lanes, to Lindblad resonance rings, tidal arcs around interacting galaxies, gaseous shells and rings in galactic disks, and molecular clouds at the edges of HII regions. The role of compression is either to bring some amount of otherwise stable gas together so it can collapse and form stars on its own, or to compress an existing cloud from a stable configuration to an unstable configuration, at which point it, too, forms stars on its own. Always accompanying this gas redistribution or compression is an enhancement in internal energy dissipation. Otherwise, the region would have collapsed into stars on its own. Compression through a shock does this reduction, or compression-enhancement of magnetic diffusion, or even compression to reduce the turbulent dissipation time. Without compression, the region may still collapse on its own, but with a longer time scale.

Because the final step in all of these triggering scenarios is the formation of stars deep in a cloud core, away from any pressure source that may be acting on the cloud surface, the detailed processes of star formation, such as stellar collapse, accretion, disk formation, and so on, should not depend much on triggering. If the source of compression also heats the gas, then perhaps the thermal Jeans mass increases in the compressed region, and this might affect the stellar initial mass function. However, higher driving luminosities and therefore higher cloud temperatures are usually accompanied by higher pressures in a way that the thermal Jeans mass stays about constant (Elmegreen et al., 2008).

The overall affect of triggered star formation on the average star formation rate seems to be small in the main parts of galaxy disks. The empirical laws discussed

in Lecture 1 seem not to depend on how the self-gravitating molecular gas is made, as long as it is made quickly between previous molecular cloud disruptions. If the dispersed gas from a previous event of star formation lingers around in a diffuse state for a long time, without forming stars, then it might still turn molecular from self-shielding, thereby contributing to $\Sigma_{\rm H2}$, but not contribute in the right proportion to $\Sigma_{\rm SFR}$. The empirical Bigiel et al. (2008) law would then fail. We suggested in Lecture 2 that this may be the case for dust clouds in the interarm regions of M51, i.e., that they are marginally stable to have lasted so long from their formation in the previous spiral arm. But the fraction of molecules in a non-gravitating form cannot be large for the correlation between $\Sigma_{\rm SFR}$ and $\Sigma_{\rm H2}$ to work out as well as it does. Frequent gas compression by all of the various pressures in the ISM, combined with the forced loss of internal energy that accompanies this compression, ensures that most of the molecular and atomic debris from one event of star formation soon makes it into another event of star formation. Prevalent triggering thereby acts as a scavenger for inert diffuse clouds, keeping most parts of the ISM in a constant state of collapse or imminent collapse. This is the saturation in star formation that previous lectures have mentioned.

With very low star formation rates, as in dwarf galaxies and the outer parts of disks, a much higher fraction of the gas can be in diffuse form, and then triggering can play a more direct role in the average star formation rate. At a very minimum, it can provide locally high pressures where the thermal stability of the gas allows a cool phase to exist in equilibrium with the radiation field. Without such cool phases, disk instabilities will just make warm and diffuse flocculent spirals in the gas, and there will not be enough dense matter to affect the star formation rate. Put simply, at very low average pressures, cool diffuse clouds seem to require pressure disturbances for their formation from the warm phase. Most commonly, outer spiral arms seem to do this, but stellar pressure sources might be important too. This enablement of cool cloud formation is presumably the first step in the condensation process that leads to star formation.

References

Beerer, I.M. 2010, ApJ, 720, 679

Beltrán, M. T., Massi, F., López, R., Girart, J. M., & Estalella, R. 2009, A&A, 504, 97

Bertoldi, F., & McKee, C.F. 1990, ApJ, 354, 529

Bigiel, F., Leroy, A., Walter, F., Brinks, E., de Blok, W. J. G., Madore, B., & Thornley, M. D. 2008, AJ, 136, 2846

Breitschwerdt, D., & de Avillez, M. A. 2006, A&A, 452, L1

Castor, J., McCray, R., & Weaver, R 1975, ApJ, 200, L107

Choudhury, R., Mookerjea, B., & Bhatt, H. C. 2010, ApJ, 717, 1097

Connon et al. 2005, ApJ, 630, L37

Dale, J. E., Bonnell, I. A., Clarke, C. J., & Bate, M. R. 2005, MNRAS, 358, 291

Dale, J. E., Bonnell, I. A., & Whitworth, A. P. 2007a, MNRAS, 375, 1291

Dale, J. E., Clark, P. C., & Bonnell, I. A. 2007b, MNRAS, 377, 535

de Geus, E. 1992, A&A, 262, 258

Deharveng, L., Schuller, F., Anderson, L. D., Zavagno, A., Wyrowski, F., Menten, K. M., Bronfman, L., Testi, L., Walmsley, C. M., & Wienen, M. 2010, arXiv1008.0926

Deharveng, L., Lefloch, B., Massi, F., Brand, J., Kurtz, S., Zavagno, A., & Caplan, J. 2006, A&A, 458, 191

Desai, K.M. 2010, AJ, 140, 584

Efremov, Yu.N., & Elmegreen, B.G. 1998, MNRAS, 299, 643

Ehlerová, S., & Palouš, J. 2005, A&A, 437, 101

Elmegreen, B.G. 1989, ApJ, 340, 786

Elmegreen, B.G. 1994, ApJ, 427, 384

Elmegreen, B. G., Palouš, J., & Ehlerová, S. 2002, MNRAS, 334, 693

Elmegreen, B.G., Klessen, R., & Wilson, C. 2008, ApJ, 681, 365

Fukuda, N., Hanawa, T., Sugitani, K. 2002, ApJ, 568, L127

Getman, K.V., Feigelson, E.D., Garmire, G., Broos, P., & Wang, J. 2007, ApJ, 654, 316

Goudis, C., Meaburn, J. 1978, A&A, 68, 189

Gritschneder, M., Naab, T., Walch, S., Burkert, A., & Heitsch, F. 2009, ApJ, 694, L26

Guarcello, M. G., Micela, G., Peres, G., Prisinzano, L., & Sciortino, S. 2010, A&A, 521, 61

Hosokawa, T., & Inutsuka, S-I. 2005, ApJ, 623, 917

Hosokawa, T., & Inutsuka, S-I. 2006a, ApJ, 646, 240

Hosokawa, T., & Inutsuka, S-I. 2006b, ApJL, 648, 131

Hosokawa, T. & Inutsuka, S.-I. 2007, ApJ, 664, 363

Indebetouw, R., Robitaille, T. P., Whitney, B. A., Churchwell, E., Babler, B., Meade, M., Watson, C., & Wolfire, M. 2007, ApJ, 666, 321

Kim, J., Balsara, D., & Mac Low, M.-M. 2001, JKAS, 34, 333

Kirk, J. M., Ward-Thompson, D., & André, P. 2005, MNRAS, 360, 1506

Klein, R.I., Sandford, M.T., & Whitaker, R.W. 1980, Space Sci. Rev. 27, 275

Könyves, V., Kiss, Cs., Moór, A., Kiss, Z. T., & Tóth, L. V. 2007, A&A, 463, 1227

Lada, C.J., Alves, J., & Lada, E.A. 1999, ApJ, 512, 250

Lallement, R., Welsh, B. Y., Vergely, J. L., Crifo, F., & Sfeir, D. 2003, A&A, 411, 447

Lombardi, M., Lada, C. J., & Alves, J. 2008, A&A, 489, 143

McKee, C.F. 1989, ApJ, 345, 782

McKibben Nail V., & Shapley H., 1953, Harvard Rep. 373

Mellema, G., Arthur, S.J., Henney, W.J., Iliev, I.T., & Shapiro, P.R. 2006, ApJ, 647, 397

Miao, J., White, G.J., Nelson, R., Thompson, M., & Morgan, L. 2006, MNRAS, 369, 143

Patel, N.A., Goldsmith, P.F., Snell, R.L., Hezel, T., & Xie, T. 1995, ApJ, 447, 721

Reach, W.T., et al. 2009, ApJ, 690, 683

Smith, N. 2010, MNRAS, 406, 952

Snowden, S., Egger, R., Finkbeiner, D. P., Freyberg, M. J., & Plueinsky, P. P. 1998, ApJ, 493, 715

Spitzer, L. Jr., 1978, in *Physical Processes in the Interstellar Medium*, New York: Wiley,

Sugitani, K., Fukui, Y., Mizuni, A., & Ohashi, N. 1989, ApJL, 342, 87

Sugitani, K., Tamura, M., & Ogura, K. 1995, ApJL, 455, 39

Sugitani, K., et al. 2002, ApJ, 565, L25

Yamaguchi, R., Mizuno, N., Onishi, T., Mizuno, A., Fukui, Y. 2001, ApJ, 553, L185

Walborn, N.R., Maíz-Apellániz, J., & Barbá, R.H. 2002, AJ, 124, 1601

Walter, F., & Brinks, E. 1999, AJ, 118, 273

Whitworth A. P., Bhattal A. S., Chapman S. J., Disney M. J., & Turner J. A., 1994, MNRAS, 268, 291

Wilcots, E.M., & Miller, B.W. 1998, AJ, 116, 2363

Wünsch, R., Dale, J. E., Palouš, J., & Whitworth, A. P. 2010, MNRAS, 407, 1963

Zavagno, A., Deharveng, L., Comerón, F., Brand, J., Massi, F., Caplan, J., & Russeil, D. 2006, A&A, 446, 171

Ecole Evry Schatzman 2010: Star Formation in the Local Universe
Eds. C. Charbonnel & T. Montmerle
EAS Publications Series, 2011

STAR FORMATION DURING GALAXY FORMATION

Bruce G. Elmegreen[1]

Abstract. Young galaxies are clumpy, gas-rich, and highly turbulent. Star formation appears to occur by gravitational instabilities in galactic disks. The high dispersion makes the clumps massive and the disks thick. The star formation rate should be comparable to the gas accretion rate of the whole galaxy, because star formation is usually rapid and the gas would be depleted quickly otherwise. The empirical laws for star formation found locally hold at redshifts around 2, although the molecular gas consumption time appears to be smaller, and mergers appear to form stars with a slightly higher efficiency than the majority of disk galaxies.

1 Introduction

In the first four lectures of this series, we reviewed star formation in local galaxies. Recall that the star formation rate is proportional to the CO emission, from which we concluded that star formation occurs only in molecular gas and that the consumption rate from molecules to gas is constant. This derivation assumed a fixed CO to H_2 conversion rate to get the molecular gas mass, a fixed IMF, uniform grain properties, and certain extinction corrections to get the star formation rate. In addition, the molecular fraction scales almost linearly with pressure, and the pressure depends on the mass column densities, $\Sigma_{\rm gas}$ and $\Sigma_{\rm stars}$, and the velocity dispersions, $\sigma_{\rm gas}$ and $\sigma_{\rm stars}$. We also saw that spiral waves promote star formation in the arms, or organize the star formation, but do not affect the average rate much. The same is apparently true for star formation in shells, bright rims and pillars, which trigger star formation in these regions, i.e., organize where it happens, without changing the global average rate much. Star formation seems saturated in inner disks, so the detailed mechanisms of cloud formation do not appear to matter.

[1] IBM T. J. Watson Research Center, 1101 Kitchawan Road, Yorktown Heights, New York 10598 USA, bge@us.ibm.com

DOI: (will be inserted later)

In addition, we saw that stars form in hierarchical patterns with star complexes, OB associations, clusters, and so on, because of turbulence compression and self-gravity. As a result, there are power-law mass functions for clouds, clusters, and stars, and there are space-time correlations for clusters. There are probably similar space-time correlations for young stars which are not observed yet.

We would like to discuss here what changes for young galaxies at high redshift. At first, we expect high redshift galaxies to look like normal galaxies viewed in the restframe ultraviolet. They would look dimmer because of cosmological surface brightness dimming, and the star formation regions would be blurred out because of poor spatial resolution. But still, we might expect to see the uv restframe versions of normal galactic features, i.e., exponential disks, spiral arms, bars, lots of small star-forming regions, and a general diversity in the relative prominence of disks and spheroids (i.e., the Hubble types).

Barden, Jahnke & Häussler (2008) made model images of redshifted SDSS galaxies to $z = 0.15, 0.5$, and 1, and even increased the intrinsic brightness for the $z = 1$ images. The result was a significant loss of faint structures, including the outer disk and the faint star-forming regions. Overzier et al. (2010) redshifted "Lyman Break Analogs" to $z = 2, 3$, and 4. They found that small clumps blend together and faint peripheral tidal features disappear. Petty et al. (2009) looked at the standard structural measures: the Gini coefficient, M20 (central concentration), and the Sersic index for redshifted local galaxies. They found that the model galaxies were smoother (lower Gini) and more centrally concentrated (lower M20) than their local counterparts. These studies reinforce our notion that high redshift galaxies should look somewhat smooth and centrally concentrated if they are at all like local galaxies.

In fact, when deep high resolution images of the sky were taken, particularly by the Hubble Space Telescope (HST), disk galaxies did not look anything like these expectations from local galaxies. Beyond $z \sim 2$, galaxies are mostly irregular, asymmetric, and clumpy (van den Bergh et al., 1996; Abraham et al., 1996; Conselice et al., 2005). In particular, there is a class of galaxies that is almost entirely clumpy, with nearly half of the light in several big star-forming clumps and no obvious underlying exponential disk (Elmegreen & Elmegreen, 2005). Figure 1 shows two examples of clumpy disks, with UDF catalog numbers indicated. On the left are SkyWalker[1] images using the ACS camera and on the right are NICMOS images in the near-infrared with 3× lower resolution. The galaxies contain several large star-forming clumps with no central concentration from a bulge or exponential disk.

In a catalog of galaxy morphologies in the HST Ultra Deep Field, considering only galaxies larger than 10 pixels so their internal structure can be observed, Elmegreen et al. (2005a) recognized 6 basic types: Chain galaxies (121 examples), Clump Clusters (192), Double (134), Tadpole (114), Spiral (313), and Elliptical (129). Only the spirals and ellipticals resemble local galaxies, and even then

[1]designed by K. Jahnke and S.F. Sánchez, AIP 2004

the spirals tend to have bigger star-forming regions than local spirals and the ellipticals are clumpy as well (Elmegreen et al., 2005b). Photometric redshifts of these galaxies (Elmegreen et al., 2007a) suggested that all of the clumpy types extend out to at least $z \sim 5$ with extreme starburst spectral energy distributions. The spirals and ellipticals end at about $z \sim 1.5$, which could be because either their number density drops, or they are too faint in the restframe uv to see at higher redshifts.

2 What are the Clumpy Types?

Chain galaxies were originally identified by Cowie, Hu & Songaila (1995) using ground-based images. They are linear objects with several giant clumps along their length. There is often no central red clump, and no exponential profile as in a modern edge-on spiral galaxy. There are also many oval-shaped clumpy galaxies that resemble chains in having the same numbers, magnitudes, and colors for the clumps. More important, the relative numbers of these systems, chains versus clumpy galaxies, is consistent with the chains being edge-on clump clusters (Elmegreen et al., 2004a; Elmegreen & Elmegreen, 2005). Thus we have a new morphological type of galaxy, a thoroughly clumpy disk viewed in random

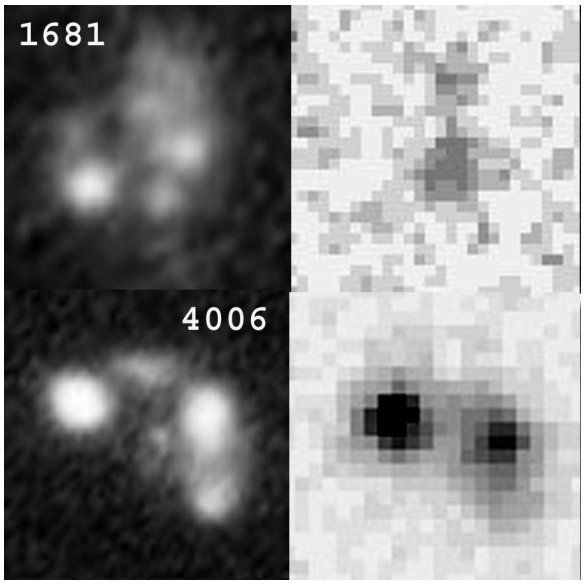

Fig. 1. Two examples of clump cluster galaxies from the HST UDF with color ACS camera images on the left and NICMOS images on the right (from Elmegreen et al., 2009a). These galaxies are characteristic of this class, having several large clumps of star formation and no obvious interclump disk.

orientations, that occurs primarily at high redshift.

Chains and clump clusters are so common that all modern spirals could have gone through this phase at $z > 1$. Essentially all observed disk systems are very clumpy at $z > 2$. The comoving space density of chains and clump clusters larger than 10 pixels in the UDF is $\sim 4 \times 10^{-3}$ Mpc^{-3} for $z < 1$, decreasing to $\sim 1 \times 10^{-3}$ Mpc^{-3} out to $z \sim 3$ or more. For spirals larger than 10 pixels in the UDF, the space density is 4×10^{-3} Mpc^{-3} for $z < 1$, but decreasing faster with z than the clumpy types, perhaps, in part, because spirals become too red to see. Considering also that the clumpy phase is probably shorter lived than the spiral phase, the prevalence of clumpy disks at high redshift seems clear.

Most clumps are not a bandshifting artifact of rest-UV normal star formation. Clumpy and spiral types are both present at low redshift. In GOODS, there are four basic types of disk galaxies: density wave spirals and flocculent spirals resembling today's galaxies, clumpy galaxies with a red disk between the clumps, and clumpy galaxies without any evident disk between the clumps. All four types span the same range of redshifts up to $z \sim 1$. There are clump clusters even at $z \sim 0.2$. This is such a low redshift that the observed V band in GOODS corresponds to a restframe passband of B band. Local spirals do not look like clump clusters in B band, so the clumpies are intrinsically different.

3 Mergers

Highly irregular massive disk galaxies in the local universe are usually mergers or interacting systems. We don't know if this is also true at high redshift. In the GOODS sample, there are clump clusters and chains at low redshift that look the same as those at high redshift in the UDF. But also in GOODS there are many examples of mergers and interactions that look like their local counterparts (Elmegreen & Elmegreen, 2006a; Elmegreen et al., 2007b). Thus normal mergers and interactions show up just fine in GOODS, and clump clusters are different. Clump clusters usually have no tidal features, for example, and they do not typically have double red nuclei from formerly separate galaxies.

Mergers are also not required to make a galaxy lopsided. Internal processes can do that too. Bournaud et al. (2008) observed a lopsided clump cluster in the UDF with Sinfoni. They found that it has a smooth rotation profile and metallicity gradient, so it does not look like a chaotic merger or have a double rotation curve. A simulation of this system reproduced the lopsided shape very well if the initial disk and halo were offset from each other a little. This offset seems reasonable if very young galaxies undergo rapid accretion from a cosmological inflow; they should often have their disk center-of-mass at a slightly different position than their halo center-of-mass. The disk mass in this model was 6×10^{10} $M_\odot$, with half of the disk mass in gas.

The final piece of evidence that chains are edge-on clump clusters is that the clumps in chain galaxies are highly confined to the midplanes. Their resolution-corrected rms deviation from the midplane of the chains is less than 100 pc (Elmegreen & Elmegreen, 2006b). This requires *in situ* clump formation, not

extra-galactic clump accretion. Also some chains are curved and not straight, and the clumps in them follow the curvature too, without significant deviations (Elmegreen & Elmegreen, 2006a). These may be interacting edge-on clumpy galaxies, but still the clumps formed in them and are not separate merger remnants.

4 Clump Cluster Properties

Clumpy young galaxies, whether somewhat face-on and called "clump clusters," or edge-on and called chains, have properties that are consistent with their youth, and also show variations that are consistent with their gradual evolution into modern disks.

Their youthful appearance is reinforced by the observation that they are highly molecular (Tacconi et al., 2010; Daddi et al., 2008, 2010a) and highly turbulent (Förster Schreiber et al., 2009; Law et al., 2009, see below). Presumably the turbulence is a result of energy gained from intergalactic accretion (Elmegreen & Burkert, 2010) and gravitational instabilities in the disk (Bournaud, Elmegreen & Martig, 2009). Many young galaxies have a ratio of rotation speed to twice the dispersion speed that is less than unity. Förster Schreiber et al. (2009) consider that when this ratio is less than 0.4, the disks are dispersion-dominated. Their galaxies have stellar masses in the range from 10^{10} $M_\odot$ to 10^{11} $M_\odot$ and dynamical masses that are 3 to 5 times larger, on average.

Tacconi et al. (2010) made CO (3-2) maps of several clump clusters and found that typical clumps in these galaxies have 5×10^9 $M_\odot$ of H_2 with radii $<$ 1-2 kpc, $\Sigma_{H2} = 300 - 700$ $M_\odot$ pc^{-2}, and $\sigma \sim 19$ km s^{-1}. They also derived a high gas fraction in the disks. Daddi et al. (2010a) observed CO in 6 galaxies at $z \sim 1.5$, finding rotation in some cases and a generally high gas fraction. The timescales for gas consumption, stellar build-up, and galactic dynamics were all comparable in the Daddi et al. study, which implies that the galaxies are very young. Daddi et al. also found that the efficiency of star formation is about the same as in normal galaxies today.

The clump stellar masses in clump clusters are ~ 100 times larger than star complex masses in modern spiral galaxies of similar luminosities (Elmegreen et al., 2009b). Bulges or bulge-like objects in clump clusters and chains are sometimes observed, and they are more like the clumps in terms of mass and age than are the bulges in spiral galaxies (Elmegreen et al., 2009a). The interclump surface density and age relative to the clump surface density and age also show variations among different clump clusters (Elmegreen et al., 2009b). All of these variations suggest an evolution from highly clumpy, bulge-free galaxies to smooth spiral galaxies with bulges.

There are essentially no barred clump cluster galaxies. Even if bars were present, they could hardly be recognized in such irregular disks. Bars appear only when the galaxies calm down and develop exponential disks and central concentrations or bulges. Still, there are elongated clumps in some clump clusters, suggesting protobars (Elmegreen et al., 2004b). If these objects really turn into bars, then this suggests bar formation can be a gas-rich process, including signif-

icant energy dissipation, and not a pure stellar process as in standard numerical models.

5 Working Model

The most likely model for the origin of clumps in clumpy galaxies is that they form by gravitational instabilities in rapidly assembled disks. The clumps are confined to within 100 pc of the mean disk, they are young star-forming regions (not diverse merged galaxies), the clump masses are 10^7 $M_\odot$ – 10^8 $M_\odot$, sometimes 10^9 $M_\odot$, and these masses appear to be the ISM Jeans masses with the measured turbulent speeds and gas column densities. For example, $M_{\rm Jeans} \sim \sigma^4/G^2\Sigma \sim 10^8$ $M_\odot$ if $\sigma \sim 30$–50 km s^{-1} and $\Sigma_{\rm gas} \sim 100$ $M_\odot$ pc^{-2}. These dispersions are consistent with observed HII dispersions (Förster-Schreiber et al., 2006; Förster Schreiber et al., 2009; Weiner et al., 2006; Genzel et al., 2006, 2008; Puech et al., 2007; Law et al., 2009) and this column density is typical for the inner disk regions of spiral galaxies today. It is also comparable to what Tacconi et al. (2010) observed directly using CO emission.

There are many consequences of having such large clumps in a galaxy disk (Noguchi, 1999; Immeli et al., 2004a,b; Bournaud, Elmegreen & Elmegreen, 2007). They contribute strongly to the total disk potential, so they interact gravitationally, experience strong dynamical friction, and lose angular momentum to the outer disk. This all causes them to migrate rather quickly to the disk center where they contribute to a growing bulge (Elmegreen et al., 2008a). Star formation in the center can get triggered by their merger too, and this adds to the bulge. At the same time, their disruption in the disk causes it to smooth out, and this, combined with their angular momentum transfer, gives the disk an exponential radial profile (Bournaud, Elmegreen & Elmegreen, 2007). All of this disk evolution can happen within 0.5-1 Gyr.

Stirring from the clumps also thickens the disk and this probably produces the thick disk component of today's spiral galaxies (Bournaud, Elmegreen & Martig, 2009). Thick disks can also form by minor mergers, both through the stirring of existing disk stars and the dispersal of the merger remnants (Quinn et al., 1993; Walker et al., 1996). However, thick disks formed in this way flare out at the edge, and real thick disks do not seem to do this (Yoachim & Dalcanton, 2006; Bournaud & Elmegreen, 2009). Stirring by internal processes automatically makes a thick disk with an approximately constant scale height, because the stirring force from clump gravity is proportional to the disk restoring force from gravity. In the case of a merger, the stirring force is proportional to the companion galaxy mass and independent of disk restoring force, so the disk is dispersed much further in the outer regions than the inner regions (Bournaud & Elmegreen, 2009).

There is also a possible connection with nuclear black holes if the dense clusters that are likely to be present in the cores of the individual disk clumps form intermediate mass black holes by stellar coalescence, as proposed for dense clusters by Ebisuzaki et al. (2001), Portegies-Zwart & McMillan (2002), and others. If the clumps form black holes in this way, then these black holes will migrate

into the disk center along with the clumps, and possibly merge to make a massive nuclear black hole. Simulations of this process obtain a correlation between the black hole mass and the bulge velocity dispersion that is similar to what is observed (Elmegreen et al., 2008b). If the clumps make globular clusters too (Shapiro et al., 2010), then the correlation between globular cluster number and central black hole mass (Burkert & Tremaine, 2010) might be explained in the same way.

6 Stream-fed Disks

Galaxy accretion by cold gas streams is a way to feed gas into the disks fast enough to produce wild instabilities and clump formation. This can all happen without galaxy mergers, except for some small galaxy-like pieces that come in with the cold flows. The recognition of cold flows is a major change in thinking about how galaxies form (Murali et al., 2002; Birnboim & Dekel, 2003; Semelin & Combes, 2005; Dekel & Birnboim, 2006; Ocvirk et al., 2008; Dekel et al., 2009a,b; Agertz et al., 2009; Kereŝ et al., 2005, 2009; Brooks et al., 2009). Hierarchical build-up models in the cold dark matter scenario may not apply to baryons as much as they apply to cold dark matter itself. The baryons may enter a galaxy in the form of cold flows, rather than minor and major mergers of component galaxies, each with their own dark matter halo.

Ceverino, Dekel & Bournaud (2010) modeled cold and hot flows with a disk galaxy forming in the center. The model is appropriate for a redshift of $z = 2.3$. They follow the formation and evolution of individual clumps in the disk gas, showing how the accretion quickly makes an unstable gas disk, which forms giant clumps that migrate to the center.

7 Local analogs of clumpy galaxies

Clumpy galaxies do not look like local galaxies even when the local galaxies are modified to appear as they would at high redshift. FUV images of local galaxies contain too many star-forming clumps, and they are also more centrally concentrated than clump clusters. Spiral and barred structure in local galaxies would still show up at high redshift too (using the HST ACS camera, for example), if the disk is not too faint to see.

UDF clump clusters have bigger and fewer clumps than local galaxies, even in the restframe uv, they have no symmetry or central concentration, and they are much brighter in restframe magnitudes. Typical clump clusters have surface brightnesses that are more than 10 times larger than the surface brightness of, for example, M101, which is a locally bright galaxy with lots of giant star-formation clumps (although the M101 clumps are still small by high redshift standards).

We may wonder if local flocculent spiral galaxies are a better match to high-z galaxies because local flocculents get most of their structure from gravitational instabilities in the gas and there are no prominent spiral waves in the old stellar disk. Two redshifted versions of the flocculent galaxy NGC 7793 were shown in

Elmegreen et al. (2009b) and compared to GEMS galaxies. The local and distant galaxies do not look similar at all. In general, local galaxies are too smooth and too centrally concentrated compared to clump clusters.

On the other hand, a local dwarf Irregular galaxy is a good match to a clump cluster, although the clump clusters are much more massive (Elmegreen et al., 2009b). Clump clusters resemble local dwarf irregulars because both have high gas fractions, both have big complexes relative to the galaxy size, both have relatively thick disks, and both have high velocity dispersions relative to the rotation speed. Recall that $L_{\rm Jeans}/{\rm GalaxySize} \sim H_{\rm disk}/{\rm GalaxySize} \sim (\sigma/V)^2$. That is, the clump size from gravitational instabilities is comparable to the galactic scale height, and the ratio of these lengths to the galaxy size is the square of the ratio of the velocity dispersion to the rotation speed. Thus big complexes, thick disks, and high dispersions (relative to galaxy size and rotation speed) all go together regardless of the galaxy mass.

Both local dwarf irregulars and clump clusters are irregular because they have a relatively high gas mass and a high σ/V. Both are also relatively young in terms of the number of rotations they have lived and in terms of the relative gas abundance. The resemblance between clump clusters and local dwarfs is another example of down sizing: small galaxies today (dwarf irregulars) are doing what big galaxies (clump clusters) did at $z \sim 2$ (Elmegreen et al., 2009b).

There are other local galaxies that resemble clump clusters too, but they have about the same stellar mass as clump clusters, i.e., they are large galaxies. These local analogues are extremely rare, however. Casini & Heidmann (1976a,b) and Maehara et al. (1988) discovered local "clumpy irregular galaxies" of normal size. Examples are Markarian 296, 325, 7, 8 (which are ultraviolet galaxies), and Kiso UV excess galaxies 1618+378, 1624+404, 1626+413, and Mrk 297. Maehara et al. (1988) determined galactic distances of 60 to 120 Mpc, clump sizes of $\sim 2''$ (corresponding to 1 kpc), and clump absolute magnitudes of $M_{\rm B} \sim -11$ to -16 mag (corresponding to $\sim 10^6\ L_\odot$ to $10^8\ L_\odot$).

Garland et al. (2007) studied Luminous Compact Blue Galaxies. These are small, high luminosity, high surface brightness galaxies with a blue color. They are also gas-rich (CO, HI), like high-z galaxies, and rotating with distorted velocities, as if they are interacting or lopsided. Overzier et al. (2008, 2009, 2010) studied Lyman Break Analogs (Heckman, 2005). These are super-compact uv-luminous galaxies. They are GALEX objects with $L_{\rm FUV} > 10^{10.3}\ L_\odot$ and intensities $I_{\rm FUV} > 10^9\ L_\odot\ {\rm kpc}^{-2}$ at redshifts $z < 0.3$. They are also very rare ($\sim 10^{-6}\ {\rm Mpc}^{-3}$).

8 What should a Model of Star Formation be for High Redshift Galaxies?

Young galaxies look like their whole disk is out of equilibrium. In general terms, the star formation rate is expected to equal the accretion rate. This implies that if simple laws like the KS relation or the Bigiel-Leroy relation apply, then they fix the gas column density or molecular column density for a given star formation rate, not the other way around. Maybe the molecular abundance still depends

on pressure and the radiation field, and maybe stars still form only in molecular gas, but if the star formation rate is pinned to the accretion rate, then these local relations are not useful and in predicting the star formation rate. Perhaps the growth rate of GMCs equals the accretion rate by a whole galaxy. This would seem to be necessary to maintain a steady state. In a broad sense, this situation is like the dynamical triggering models discussed in these Lectures earlier, i.e., the spiral-wave or shell-like organization of gas into star-forming regions. Instead of spiral waves and shells collecting matter on a kpc scale, whole galaxies are collecting matter on a 10 kpc scale.

9 Comparison of Star Formation Models

Choi & Nagamine (2010) compared three models for star formation in cosmological simulations, the Springel & Hernquist (2003) model, the Blitz & Rosolowsky (2006) model, and the Schaye & Dalla Vecchia (2008) model. These are instructive to review here so that the diversity of analytical models can be noted.

In the Springel & Hernquist (2003) model, there is cooling gas with a star formation rate

$$d\rho_*/dt = (1-\beta)\rho_c/t_{\rm SFR}, \tag{9.1}$$

where β equals the supernova gas return fraction, ρ_c equals the density of cool clouds, $t_{\rm SFR} = t_0^*(\rho/\rho_{\rm th})^{-1/2}$ is the dynamical time, where $t_0^* = 2.1$ Gyr gives the local KS law. They also assumed $\Sigma_{\rm SFR} = 0$ if $\Sigma < \Sigma_{\rm th}$ for threshold column density $\Sigma_{\rm th}$, and $\Sigma_{\rm SFR} = A(\Sigma_{\rm gas}/1\ M_\odot\ {\rm pc}^2)^n$ for $A = 2.5 \pm 0.7\ M_\odot\ {\rm yr}^{-1}\ {\rm kpc}^{-2}$, $n = 1.4$, and $\Sigma_{\rm th} = 10\ M_\odot\ {\rm pc}^{-2}$. This equation for star formation rate is combined with another equation for the rate of change of the cool cloud density,

$$d\rho_c/dt = C\beta\rho_c/t^*, \tag{9.2}$$

where $C = C_0(\rho/\rho_{\rm th})^{-4/5}$. This assumes that supernovae evaporate and form cold clouds as in McKee & Ostriker (1977).

In the Blitz & Rosolowsky (2006) model, the molecular fraction is given by $\rho_{\rm H2}/\rho_{\rm HI} = (P_{\rm ext}/P_0)^{0.92}$, where $P_0 = 4.3\times10^4\ {\rm k_B\ K\ cm^{-3}}$. Then for a star formation rate, they assume

$$d\rho_*/dt = (\rho_{\rm gas}/{\rm Gyr})/[1+(P+P_0/P_{\rm ext})^{0.92}], \tag{9.3}$$

which assumes $\Sigma \propto \rho$ (a constant scale height). This star formation rate was applied only when $P_{\rm ext} < P_0$. For $P_{\rm ext} > P_0$, Choi & Nagamine (2010) used the Springel & Hernquist law (i.e., the Kennicutt $n = 1.4$ law).

The third model was that of Schaye & Dalla Vecchia (2008). These authors solved for the scale height using $\Sigma_{\rm gas} = \rho_{\rm gas}L_{\rm Jeans} = (\gamma f_{\rm g}P_{\rm tot}/G)^{1/2}$, where γ is the adiabatic index: $P_{\rm tot} \sim \rho_{\rm gas}^\gamma$ ($P_{\rm tot}$ and $\rho_{\rm tot}$ include stars), $f_{\rm g}$ equals the gas mass fraction, and $f_{\rm th}$ equals the thermal pressure fraction ($P = f_{\rm th}P_{\rm tot}$). They assumed $f_{\rm g} = f_{\rm th}$, so if $\Sigma_{\rm SFR} = A\Sigma_{\rm gas}^n = \Sigma_{\rm gas}/t$ which means $t = \Sigma_{\rm gas}^{1-n}/A$, then $t_{\rm SFR} = A^{-1}(M\ \odot\ {\rm pc}^2)^n(\gamma P/G)^{(1-n)/2}$, and finally $d\rho_*/dt = \rho_{\rm gas}/t_{\rm SFR}$. Note

that in this model, $\Sigma_{\rm SFR} \propto \Sigma_{\rm gas} P^{0.2}$. They also assumed a threshold density, $\rho_{\rm th} = \Sigma_{\rm th}/L_{\rm Jeans}$, so $\rho_{\rm th} = \Sigma_{\rm th}^2 G/c_{\rm s}^2 f_{\rm g}$ for $c_{\rm s} = 1.8$ km s^{-1} (500K gas), and they assumed $P = K\rho^{4/3}$.

Choi & Nagamine (2010) note that the Springel & Hernquist model forms too many stars at low $\Sigma_{\rm gas}$ and this causes it to form stars too early in the Universe. The other models have a pressure dependence for star formation which gives an acceptably low rate in low pressure regions.

Genzel et al. (2010) reviewed the star formation and CO data for high-z galaxies in the context of the "main-sequence line" for star formation:

$$SFR(M_\odot \ {\rm yr}^{-1}) = 150(M_*/10^{11} \ M_\odot)^{0.8}([1+z]/3.2)^{2.7} \tag{9.4}$$

(Bouche et al., 2010; Noeske et al., 2007; Daddi et al., 2007).

Genzel et al. noted that the gas depletion time depends weakly on z. It is ~ 0.5 Gyr at $z > 1$, and 1.7 Gyr at $z = 0$, while mergers have $2.5 - 7.5\times$ shorter depletion times than non-mergers. At $z > 1$, the depletion time is comparable to the stellar age, and it is always shorter than the Hubble time. This means there is a continuous need for gas replenishment in galaxy disks.

Genzel et al. also found that the molecular star formation-column density relation is in agreement with Bigiel et al. (2008). There is no steepening at $\Sigma_{\rm gas} > 100 \ M_\odot$ pc^{-2} like there appears to be in local starbursts. In general, they find no variation in the empirical star formation law with redshift.

The dynamical version of the Kennicutt (1998) relation was examined by Genzel et al. too. The dynamical relation says that the star formation rate is proportional to the gas column density divided by the local orbit time. Even in this form, mergers were found to be more efficient at star formation than non-mergers. The star formation efficiency per unit dynamical time was about 1.7%.

These considerations led Genzel et al. to a fundamental plane of star formation, in which the total galactic star formation rate depends only on the dynamical time and the total molecular mass:

$$\log\left(\frac{SFR}{M_\odot/{\rm yr}}\right) = -0.78 \pm 0.23 \log\left(\frac{t_{\rm dyn}}{\rm yr}\right) + 1.37 \pm 0.16 \log\left(\frac{M_{\rm mol}}{M_\odot}\right) - 6.9 \pm 1.9, \tag{9.5}$$

all with a standard deviation of 0.47 dex. This is the same as

$$SFR = 130 \left(\frac{M_{\rm mol}}{10^{10} \ M_\odot}\right)^{1.37} \left(\frac{t_{\rm dyn}}{100{\rm Myr}}\right)^{-0.78} M_\odot \ {\rm yr}^{-1}. \tag{9.6}$$

Genzel et al. (2010) summarized the various star formation-density laws as follows. The Kennicutt slope of ~ 1.4 includes HI, whereas the Bigiel et al. (2008) slope of ~ 1 is just for CO (or H_2). Genzel et al. redid the Kennicutt (1998) slope of 1.4 with just H_2 and got a slope of ~ 1.33. They redid their own relation for $\Sigma_{\rm SFR}$ versus $\Sigma_{\rm gas}$ including HI in addition to H_2 and found that it increases the slope from 1.17 to 1.28. Kennicutt (1998) used the same CO-H_2 conversion factor everywhere. When Genzel et al. redid the Kennicutt (1998) data with

a variable CO-H_2 conversion factor including only H_2, the slope increased from 1.33 to 1.42. Thus the inclusion of HI and the constant CO-H_2 conversion factor somewhat cancel each other in the Kennicutt (1998) relation. Genzel et al. (2010) also included new merger galaxies, which flatten the slope compared to that in Kennicutt (1998). Writing the star formation rate as $\Sigma_{\rm mol}/t_{\rm dyn}$ works fairly well, including both mergers and normal galaxies at all redshifts.

Daddi et al. (2010b) fitted Ultrahigh Luminosity Infrared Galaxies (ULIRGS) and Submillimeter Wave Galaxies (SMGs) to the same star formation-column density relation if the SF law is $\Sigma_{\rm SFR} \sim \Sigma_{\rm gas}/t_{\rm dyn}$ ($t_{\rm dyn}$ is the rotation time at the outer disk radius). They suggested that the global star formation rate is proportional so $\sim (M_{\rm total\ gas}/t_{\rm dyn})^{1.42}$. High SFR galaxies consume their gas faster than a rotation time at the outer radius. This suggests that mergers are involved, or some other rapid accretion leading to centralized star formation.

10 Summary

Star formation at high redshift occurs in galaxies with high gas fractions and high turbulent speeds. The morphology is a clumpy disk without an exponential disk, bulge, or bar. There appear to be no exact local analogues, but what comes close are the dwarf Irregular galaxies, which are much lower in mass, along with very rare types called clumpy irregular galaxies, luminous compact blue galaxies, Lyman Break Analogs, etc.. All have a small number of giant star-forming regions, presumably because they are all gas-rich and highly turbulent. The main process of star formation everywhere seems to be gravitational instabilities. The clump masses are large and the rates are large because of the high turbulence and high gas mass fractions. There is a relation between the star formation rate and the galaxy mass versus redshift, called the "main sequence" line. Cosmological models have been made that fit this line fairly well. Generally, the $\Sigma_{\rm SFR}$ versus $\Sigma_{\rm mol}$ relation is similar to that in local galaxies, with a slight preference for a rate given by the galaxy dynamical time rather than the pure gas dynamical time. In galaxy accretion models, the star formation rate quickly becomes equal to the gas accretion rate. Presumably $\Sigma_{\rm mol}$ adjusts to accommodate or enforce this equilibrium.

References

Abraham, R.G., van den Bergh, S., Glazebrook, K., Ellis, R.S., Santiago, B.X., Surma, P., & Griffiths, R.E. 1996, ApJS, 107, 1

Agertz, O., Teyssier, R., Moore, B. 2009, MNRAS, 397, L64

Barden, M., Jahnke, K., & Häussler, B. 2008, ApJS, 175, 105

Bigiel, F., Leroy, A., Walter, F., Brinks, E., de Blok, W. J. G., Madore, B., & Thornley, M. D. 2008, AJ, 136, 2846

Birnboim Y., & Dekel A., 2003, MNRAS, 345, 349

Blitz, L., & Rosolowsky, E. 2006, ApJ, 650, 933

Bouche, N., et al. 2010, ApJ, 718, 1001

Bournaud, F., Elmegreen, B.G., & Elmegreen, D.M. 2007, ApJ, 670, 237

Bournaud, F., Daddi, E., Elmegreen, B.G., Elmegreen, D.M., Nesvadba, N., Vanzella, E., Di Matteo, P., Le Tiran, L., Lehnert, M., & Elbaz, D. 2008, A&A, 486, 741

Bournaud, F., & Elmegreen, B.G. 2009, ApJL, 694, 158

Bournaud, F., Elmegreen, B.G., & Martig, M. 2009, ApJ, 707, L1

Brooks, A. M., Governato, F., Quinn, T., Brook, C. B., & Wadsley, J. 2009, ApJ, 694, 396

Burkert, A., & Tremaine, S. 2010, ApJ, 720, 516

Casini, C., & Heidmann, J. 1976a, A&AS, 24, 473

Casini, C., & Heidmann, J. 1976b, A&A, 47, 371

Ceverino, D., Dekel, A., & Bournaud, F. 2010, MNRAS, 404, 2151

Choi, J.-H., & Nagamine, K. 2010, MNRAS, 407, 1464

Conselice, C. J., Blackburne, J. A., Papovich, C. 2005, ApJ, 620, 564

Cowie, L., Hu, E., & Songaila, A. 1995, AJ, 110, 1576

Daddi, E., et al. 2007, ApJ, 670, 156

Daddi, E., Dannerbauer, H., Elbaz, D., Dickinson, M., Morrison, G., Stern, D., & Ravindranath, S. 2008, ApJ, 673, L21

Daddi, E. et al. 2010a, ApJ, 713, 686

Daddi, E. et al. 2010b, ApJL, 714, L118

Dekel A., & Birnboim Y., 2006, MNRAS, 368, 2

Dekel, A., et al. 2009a, Nature, 457, 451

Dekel, A., Sari, R., & Ceverino, D. 2009b, ApJ 703, 785

Ebisuzaki, T., et al. 2001, ApJ, 562, L19

Elmegreen, B.G., Elmegreen, D.M., & Hirst, A.C. 2004b, ApJ, 612, 191

Elmegreen, B.G., Elmegreen, D.M. 2005, ApJ, 627, 632

Elmegreen, B.G., & Elmegreen, D.M. 2006b, ApJ, 650, 644

Elmegreen, B.G., Bournaud, F., & Elmegreen, D.M. 2008a, ApJ, 688, 67

Elmegreen, B.G., Bournaud, F., & Elmegreen, D.M. 2008b, ApJ, 684, 829

Elmegreen, B.G., Elmegreen, D.M., Fernandez, M.X., & Lemonias, J.J., 2009a, ApJ, 692, 12

Elmegreen, B.G., & Burkert, A. 2010, ApJ, 712, 294

Elmegreen, D.M., Elmegreen, B.G., & Hirst, A.C. 2004a, ApJ, 604, L21

Elmegreen, D.M., Elmegreen, B.G., Rubin, D.S., & Schaffer, M.A. 2005a, ApJ, 631, 85

Elmegreen, D.M., Elmegreen, B.G., & Ferguson, T.E. 2005b, ApJL, 623, L71

Elmegreen, D.M., Elmegreen, B.G. 2006a, ApJ, 651, 676

Elmegreen, D.M., Elmegreen, B.G., Ravindranath, S., & Coe, D. 2007a, ApJ, 658, 763

Elmegreen, D.M., Elmegreen, B.G., Ferguson, T., & Mullan, B. 2007b, ApJ, 663, 734

Elmegreen, D.M., Elmegreen, B.G., Marcus, M., Shahinyan, K., Yau, M., & Petersen, M. 2009b, ApJ, 701, 306

Förster-Schreiber, N. M., et al. 2006, ApJ, 645, 1062

Förster Schreiber, et al. 2009, ApJ, 706, 1364

Garland, C. A., Pisano, D. J., Williams, J. P., Guzmán, R., Castander, F. J., & Sage, L.J. 2007, ApJ, 671, 310

Genzel, R. et al. 2006, Nature, 442, 786

Genzel, R. et al. 2008, ApJ, 687, 59

Genzel, R. et al. 2010, MNRAS, 407, 2091

Heckman, T.M., 2005, ApJL ,619, 35

Immeli, A., Samland, M., Westera, P., & Gerhard, O. 2004a, ApJ, 611, 20

Immeli, A., Samland, M., Gerhard, O., & Westera, P. 2004b, A&A, 413, 547

Kennicutt, R.C., Jr. 1998, ApJ, 498, 541

Kereŝ, D., Katz, N., Weinberg, D.H., Davé, R. 2005, MNRAS, 363, 2

Kereŝ, D., Katz, N., Fardal, M., Davé, R., & Weinberg, D. H. 2009, MNRAS, 395, 160

Law, D.R., Steidel, C.C., Erb, D.K., Larkin, J.E., Pettini, M., Shapley, A.E., Wright, S.A. 2009, ApJ, 697, 2057

Maehara, H., Hamabe, M., Bottinelli, L., Gouguenheim, L., Heidmann, J., & Takase, B. 1988, PASJ, 40, 47

McKee, C. F., & Ostriker, J. P. 1977, ApJ, 218, 148

Murali, C., Katz, N., Hernquist, L., Weinberg, D.H., & Davé, R. 2002, ApJ, 571, 1

Noeske, K. G., et al. 2007, ApJ, 660, L47

Noguchi, M. 1999, ApJ, 514, 77

Ocvirk, P., Pichon, C., & Teyssier, R. 2008, MNRAS, 390, 1326

Overzier, R.A., et al. 2008, ApJ., 677, 37

Overzier, R. A. et al. 2009, ApJ, 706, 203

Overzier, R.A., Heckman, T.M., Schiminovich, D., Basu-Zych, A., Goncalves, T., Martin, D.C., & Rich, R.M. 2010, ApJ, 710, 979

Petty, S.M., de Mello, D.F., Gallagher, J.S., III, Gardner, J.P., Lotz, J.M., Mountain, C.M., & Smith, L.J. 2009, AJ, 138, 362

Portegies-Zwart, S. F., & McMillan, S. L. W. 2002, ApJ, 576, 899

Puech, M., Hammer, F., Lehnert, M. D., & Flores, H. 2007, A&A, 466, 83

Quinn, P. J., Hernquist, L., & Fullagar, D. P. 1993, ApJ, 403, 74

Schaye, J, & Dalla Vecchia, C. 2008, MNRAS, 383, 1210

Semelin, B., & Combes, F. 2005, A&A, 441, 55

Shapiro, K.L., Genzel, R., & Förster Schreiber, N.M. 2010, MNRAS, 403, L36

Springel, V., & Hernquist, L. 2003, MNRAS, 339, 289

Tacconi, L., et al. 2010, Nature, 463, 781

van den Bergh, S., Abraham, R.G., Ellis, R.S., Tanvir, N.R., Santiago, B.X., & Glazebrook, K.G. 1996, AJ 112, 359

Walker, I. R., Mihos, J. C., & Hernquist, L. 1996, ApJ, 460, 121

Weiner, B. J., et al. 2006, ApJ, 653, 1027

Yoachim, P. & Dalcanton, J. J. 2006, AJ, 131, 226